Provenance Shifts During Neogene Brahmaputra Delta Progradation Tied to Coupled Climate and Tectonic Change in the Eastern Himalaya

Paul M. Betka[1] , Stuart N. Thomson[2] , Ryan Sincavage[3] , C. Zoramthara[4] , C. Lalremruatfela[4] , Karl A. Lang[5] , Michael S. Steckler[6] , Devojit Bezbaruah[7], Pradip Borgohain[8], and Leonardo Seeber[6]

[1]Department of Atmospheric, Oceanic, and Earth Sciences, George Mason University, Fairfax, VA, USA, [2]Department of Geosciences, University of Arizona, Tucson, AZ, USA, [3]Geology Department, Radford University, Radford, VA, USA, [4]Department of Geology, Government Zitiri Residential Science College, Aizawl, India, [5]School of Earth and Atmospheric Sciences, Georgia Tech, Atlanta, GA, USA, [6]Lamont-Doherty Earth Observatory, Columbia University, Palisades, NY, USA, [7]Department of Applied Geology, Dibrugarh University, Dibrugarh, India, [8]Department of Petroleum Technology, Dibrugarh University, Dibrugarh, India

Abstract The Bengal Basin preserves the erosional signals of coupled tectonic-climatic change during late Cenozoic development of the Himalayan orogen, yet regional correlation and interpretation of these signals remains incomplete. We present a new geologic map of fluvial-deltaic deposits of the Indo-Burman Ranges (IBR), five detrital zircon fission track analyses, and twelve high-n detrital zircon U-Pb age distributions (dzUPb) from the Barail (late Eocene–early Miocene), Surma (early–late Miocene), and Tipam (late Miocene–Pliocene) Groups of the ancestral Brahmaputra delta. We use dzUPb statistical tests to correlate the IBR units with equivalent age strata throughout the Bengal Basin. An influx of trans-Himalayan sediment and the first appearance of ~50 Ma grains of the Gangdese batholith in the lower Surma Group (~18–15 Ma) records the early Miocene arrival of the ancestral Brahmaputra delta to the Bengal Basin. Contributions from Himalayan sources systematically decrease up section through the late Miocene as the contribution of Trans-Himalayan Arc sources increases. The Miocene (~18–8 Ma) deposition of the Surma Group records upstream expansion of the ancestral Brahmaputra River into southeastern Tibet. Late Miocene (<8 Ma) progradation of the fluvial part of the delta (Tipam Group) routed trans-Himalayan sediment over the shelf edge to the Nicobar Fan. We propose that Miocene progradation of the ancestral Brahmaputra delta reflects increasing rates of erosion and sea level fall during intensification of the South Asian Monsoon after the Miocene Climate Optimum, contemporaneous with a pulse of tectonic uplift of the Himalayan hinterland and Tibet.

Plain Language Summary The development of mountain topography is a balance between forces that push them up (plate tectonics) and processes of erosion which break them down (climate). The Himalayan Mountains formed over the past 50 million years and their growth is attributed to tectonic and climate interactions between the India-Asia plate collision and development of monsoon conditions over south Asia. This paper examines a nearly complete record of sedimentary rocks that were eroded from various Himalayan sources and deposited in the ancestral Brahmaputra delta between ~30 and ~5 million years ago. We present sediment age data to date and correlate the deposits, as well as identify Himalayan sources that contributed sediment to the delta. Prior to a middle Miocene warm period, most sediment was sourced from the frontal ranges of the Himalaya, like the modern Ganges watershed. After the middle Miocene, when South Asian Monsoon conditions intensified, the watershed expanded north of the Himalayan divide and delivered increasingly large proportions of sediment from Tibet, like the modern Brahmaputra watershed. Middle Miocene intensification of monsoon conditions, combined with a synchronous pulse of tectonic activity, led to a major expansion of the Brahmaputra delta, the largest depositional system on Earth today.

1. Introduction

Peripheral foreland basins and flanking remnant ocean basins preserve stratigraphic and structural records of continental collisions (Beaumont, 1981), where the rates of sediment accumulation and foredeep delta progradation depend on the erosional response to both tectonic and climatic processes (e.g., Clift & Jonell, 2021; Raymo and Ruddiman, 1992). The Siwalik, Indus, and Bengal basins of the Himalayan foreland preserve more

than 50 million years of Himalayan erosion (Garzanti, 2019; Najman, 2006) and contain unique records of climate-tectonic interactions within the frontal, western, and eastern Himalaya, respectively. The Bengal Basin, including Neogene deposits of the Indo-Burman Ranges (IBR), the modern Ganges–Brahmaputra Delta, and the Bengal-Nicobar Fan, forms the archetypal example of a source-to-sink sedimentary system in a continental collision (Graham et al., 1975; Ingersoll et al., 2003). Major Himalayan rivers, including the Brahmaputra and Ganges, have transported a copious volume ($\sim 1.1 \times 10^9$ metric tonnes/yr; Milliman and Farnsworth, 2011) of sediment to the Ganges–Brahmaputra Delta and Bengal-Nicobar Fan, recording late Cenozoic denudation of the Himalayan orogen (Curray & Moore, 1971; Curray et al., 2002; Krishna et al., 2016; Lindsay et al., 1991; Métivier et al., 1999).

The modern Bengal Basin (Figure 1) receives sediment from both the Ganges and Brahmaputra watersheds, recording denudation of both the frontal part of the Himalayan wedge (Ganges tributaries) as well as Trans-Himalayan Arc and Tibetan terranes within the modern Brahmaputra drainage area. However, mixing between these two disparate sources means they tend to homogenize discrete records of tectonic, climate, and geomorphic interactions related to development of the Himalayan orogen (e.g., Blum et al., 2018). In contrast, exhumed Neogene sedimentary rocks within the IBR primarily record the late Cenozoic progradation of the ancestral Brahmaputra delta only (Govin, Najman, Copley, et al., 2018; Sincavage et al., 2020), and thus preserve a more direct record of changes in upstream allogenic forcings related to development of the eastern Himalaya and Tibet (e.g., Lang et al., 2016; Najman et al., 2008). Over the past decade, multiple studies of IBR stratigraphy have renewed interest in the regional stratigraphic correlation of IBR sedimentary units to the more proximal Himalayan foreland sequences of the Siwalik Group (Cina et al., 2009; Chirouze et al., 2013; Govin, Najman, Copley, et al., 2018, Govin, Najman, Dupont-Nivet, et al., 2018; Lang et al., 2016) as well as the Bengal and Nicobar fans (Bergmann et al., 2020; Blum et al., 2018; Pickering, Carter, et al., 2020; Pickering, Pouderoux, et al., 2020) to reconstruct late Cenozoic changes in tectonic and climate signals within the Brahmaputra watershed. However, recognition and quantitative correlation of these signals across the middle to late Miocene depositional system is limited, with only a few prior studies of the fluvial-deltaic deposits in the IBR (Bracciali et al., 2015; Najman et al., 2008; Vadlamani et al., 2015; Yang et al., 2018) that routed sediments from the proximal foreland basin (Siwalik Group) to the Bengal-Nicobar Fan. Moreover, there is ongoing debate about the significance of observed spatial and temporal changes in the Himalayan provenance of ancestral Brahmaputra deposits with respect to the timing of major drainage reorganization within the eastern Himalaya (e.g., Allen et al., 2008; Govin, Najman, Copley, et al., 2018; Govin, Najman, Dupont-Nivet, et al., 2018; Lang et al., 2016; Sawant et al., 2017), sediment routing to the Bengal-Nicobar Fan (Blum et al., 2018; Pickering et al., 2020, Pickering, Carter, et al., 2020), and climate-tectonic feedbacks during intensification of monsoon conditions after the Miocene Climate Optimum (e.g., Betzler et al., 2018; Pickering, Carter, et al., 2020).

In this paper, we present new detrital zircon U-Pb geochronology data (dzUPb) with $n = \sim 300$ single-grain analyses per sample (i.e., high-n), and detrital zircon fission track ages (dzFT), from Oligocene to Pliocene sedimentary units of the IBR. We apply statistical tests to quantitatively correlate strata of the IBR and the eastern Himalayan Siwalik Group using previously published dzUPb data that were collected throughout the region. We further investigate temporal and spatial changes in Himalayan provenance of IBR and Siwalik stratigraphy by inverting dzUPb compilations of both bedrock Himalayan source terranes, as well as the modern Ganges and Brahmaputra river deposits, for quantitative comparison to dzUPb IBR and Siwalik basin compilations (e.g., using the method of Sundell & Saylor, 2017). Our results show statistically significant and systematic changes in sedimentary provenance between Oligocene and late Miocene deposits. The paleo-Brahmaputra watershed was draining a primarily frontal and intra-Himalayan catchment dating to at least the Oligocene. Expansion of the paleo-catchment, starting in the early Miocene (~ 18–15 Ma), is marked by initial input of trans-Himalayan sediment sourced from the Trans-Himalayan Arc and Lhasa terranes in Tibet. In the late Miocene, another increase in fluvial-deltaic sediment dispersal is accompanied by a moderate shift in zircon provenance marked by a further increase in Tibetan Trans-Himalayan Arc-derived detrital zircon. We find that the detrital zircon signatures are nearly identical in coeval deposits of the easternmost Himalayan Siwalik and IBR basins. Taken together, these deposits define a Miocene delta comparable in size ($>100,000 \text{ km}^2$) to the modern Ganges–Brahmaputra Delta. We then compare our new IBR–Siwalik results with recent dzUPb datasets from the Bengal and Nicobar Fans. We discuss several possible allogenic forcing mechanisms for early to late Miocene increased sediment mass flux, delta progradation, and delivery of Tibetan Trans-Himalayan Arc sediment to the Bengal Basin: intensification of the South Asian Monsoon after the Miocene Climate Optimum, headward expansion of the paleo-Brahmaputra river into the paleo-Yarlung river watershed, and/or increased rates of tectonically driven uplift in the eastern Himalaya.
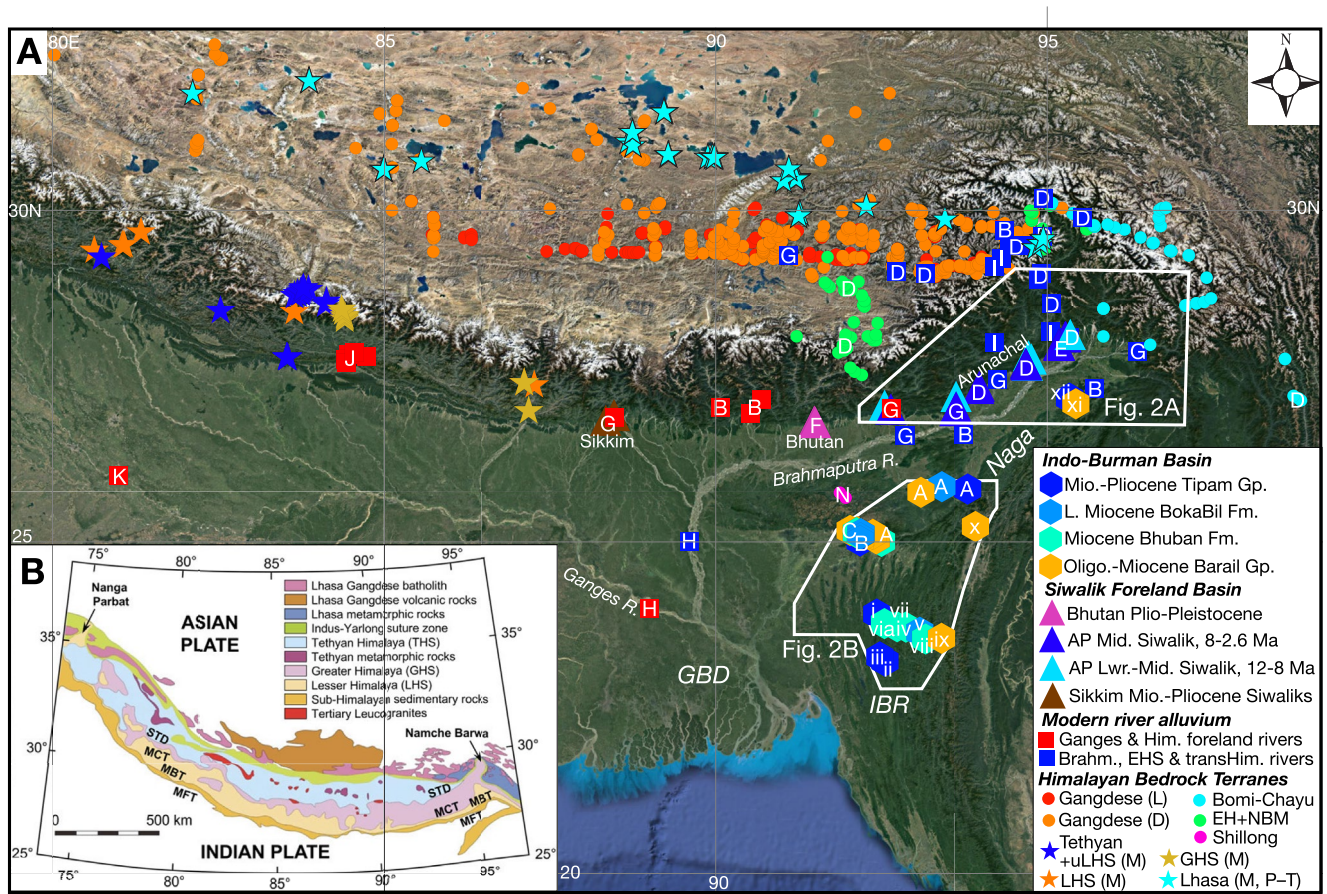
Figure 1. (a) Satellite image (Google Earth™) of the central and eastern Himalayan orogen, IBR, and Ganges–Brahmaputra Delta showing sample locations of published and new detrital zircon U-Pb age data used in this study. Data sources are as follows: i-xii, new data from this study; A, Vadlamani et al. (2015); B, Bracciali et al. (2015); C, Yang et al. (2018); D, Lang and Huntington (2014) and references in compilations therein; E, Govin, Najman, Dupont-Nivet, et al. (2018); F, Govin, Najman, Copley, et al. (2018); G, Cina et al. (2009); H, Blum et al. (2018); I, Bracciali et al. (2016); J, Amidon et al. (2005); K, Campbell et al. (2005); L, Zhu et al. (2017); M, Gehrels et al. (2011); N, Yin, Dubey, Webb, et al. (2010); O, Najman et al. (2008); P, Zhu et al. (2011); Q, Li et al. (2014); R, Guo et al. (2017); S, Hu et al. (2019); T, Q. Wang et al. (2021). (b) Map showing Himalayan tectonostratigraphic terranes (Blum et al., 2018). Abbreviations: IBR, Indo-Burman Ranges; GBD, Ganges–Brahmaputra Delta; AP, Arunachal Pradesh; EHS, eastern Himalayan syntaxis; EH, eastern Himalayas; NBM, Namche-Barwa massif; LHS, Lesser Himalayan Series; GHS, Greater Himalayan Series; uLHS, upper Lesser Himalayan series.; MFT, Main Frontal Thrust; MBT, Main Boundary Thrust; MCT, Main Central Thrust; STD, South Tibetan Detachment.

2. Geologic Background

2.1. Tectonic Setting of the IBR

The IBR extend for ∼1,000 km from the Sunda subduction zone northwards towards the eastern Himalayan syntaxis (EHS) where they are truncated by crustal faults of the Himalayan collisional orogen. Northeastward subduction of the Indian plate obliquely below the IBR is partially closing the Bay of Bengal, a remnant ocean basin (Curray & Moore, 1971; Ingersoll et al., 2003; Ni et al., 1989). This transition from subduction to collision progressed through the Neogene and is ongoing. Sediment thickness on the incoming plate increases northwards toward the Bengal Basin and the Ganges–Brahmaputra Delta. The Bengal Basin is thickest at the Ganges–Brahmaputra Delta where the IBR fold-thrust-belt widens to its maximum width of ∼300 km (Steckler et al., 2008). Active subduction accretion (Y. Wang et al., 2014) deforms the ∼16–20 km thick pile of Paleogene–Quaternary sedimentary deposits (Curray, 1991; Mitra et al., 2018; Singh et al., 2016), forming the outer- and inner-fold-thrust-belts of the IBR (Betka et al., 2018; Maurin & Rangin, 2009; Sincavage et al., 2020). The deformation front of the IBR accretionary prism is buried by Pliocene-Holocene sediments of the Ganges–Brahmaputra Delta (Figure 1; Alam et al., 2003; Najman et al., 2012; Steckler et al., 2008, 2016; Uddin and Lundberg, 1999).

Northeast of the Ganges–Brahmaputra Delta, the Burma sliver terrane converges with IBR strata that were deposited on a large promontory of the Indian basement that is now exposed in the Shillong Massif and Mikir Hills (Rangin et al., 2013). North-trending convergence between the Burma terrane and India is accommodated by active shortening in the Naga fold-thrust belt which deforms Paleogene–Neogene IBR deposits (Figures 1 and 2, Vernant et al., 2014). Ongoing convergence between the Indian and Eurasian plates also drives the southward advance of the Himalayan deformation front into the Siwalik basin (Agarwal et al., 1991; Yin, Dubey, Kelty, et al., 2010) and thick-skinned uplift of the Shillong Massif in the hanging wall of the Dauki fault (Banerjee et al., 2008; Clark & Bilham, 2008; Mallick et al., 2020). Flexural subsidence in the footwall of the Dauki Fault formed the Sylhet Basin which is filled with Plio-Quaternary fluvial-alluvial sediments (Johnson and Alam, 1991; Najman et al., 2016; Sincavage et al., 2018).

2.2. Late Cenozoic Stratigraphic Framework of the IBR

The IBR contain early Eocene to Pliocene fluvial-deltaic sediments derived from the eastern Himalaya and Tibet (Alam et al., 2003; Bracciali et al., 2015; Gani & Alam, 1999; Johnson & Alam, 1991; Sincavage et al., 2020; Vadlamani et al., 2015; Yang et al., 2018). The Neogene stratigraphy of the IBR has recently been described in terms of facies representative of modern environments on the Ganges–Brahmaputra Delta (Sincavage et al., 2020; Figures 2 and 3). The Neogene facies succession generally shows a coarsening upwards trend illustrative of the transition from shallow marine to fluvial sedimentation reflecting progradation of the ancestral Brahmaputra delta (Figure 3). The late Cenozoic IBR stratigraphy are traditionally assigned to four regionally comparable lithostratigraphic groups: the Barail, Surma, Tipam, and Dupi Tila Groups (Evans, 1932).

The Barail Group represents a late Eocene to early Miocene deep water to deltaic succession upon which the younger delta prograded from the early Miocene to Pliocene (Bezbaruah & Muzamil, 2013; Biswas & Mukhopadhyay, 2011; Sincavage et al., 2020). The Barail Group consists of interbedded silts and fine-medium sands, with bed thicknesses generally on the order of tens of centimeters up to one meter thick (Figure 3). The succession coarsens and thickens upwards overall, with some beds exhibiting convoluted and distorted bedding associated with slumps and slides along the delta front. The contact between the Barail and overlying Surma Groups is thought to be a transgressive onlap (Alam et al., 2003; Banerji, 1984). Recent magnetostratigraphic analyses of the middle and top of the Barail Group in the eastern IBR yield 29–24 Ma depositional ages, respectively (Lalremruatfela, 2020).

The Surma Group represents shallow marine conditions basinward of the subaerial delta (Alam et al., 2003) that is traditionally divided into the Bokabil and Bhuban formations for the upper and lower Surma Group, respectively. We have subdivided the Surma Group into four distinct lithofacies assemblages (Sincavage et al., 2020; Figure 3). The M1 facies consists of mm-cm scale planar laminated silty shale, interpreted as the bottomsets of the subaqueous delta (Sincavage et al., 2020). M1 grades upwards into the M2 facies, which contains alternating cyclical beds (15–20 cm thick) of cross-bedded fine sands and silts. This unit is interpreted to represent the prograding foresets of the subaqueous delta clinoform (Sincavage et al., 2020). The M3 facies is a bioturbated silty shale with cm-scale bedding exhibiting flaser, lenticular, and wavy bedding associated with sub- to intertidal depositional settings. The Surma Group is capped by the M4 facies, a thick (meter-scale beds) massive sandstone unit with occasional trough cross bedding and bi-directional current indicators (Figure 3). This unit is interpreted as tidal channels on the lower delta plain of the ancestral Brahmaputra River (Sincavage et al., 2020). Magnetostratigraphic analyses from a 1,355 m thick continuous stratigraphic section of the middle Surma Group (located just east of locality vii in Figure 2) yield depositional ages of 12.5–8 Ma and record an increase in the sediment accumulation rate from ~23 cm/ka to >39 cm/ka at ~9.5 Ma (Malsawma et al., 2010). Magnetostratigraphy constrains the depositional age for the lower Surma Group to be ~16 Ma (Lalnuntluanga et al., 2014), consistent with detrital ^{40}Ar-^{39}Ar ages reported by Uddin et al. (2010) and detrital ^{40}Ar-^{39}Ar and dzFT ages reported by Bracciali et al. (2016) that limit the lower Surma Group (Bhuban Fm.) to < 18 Ma.

Overlying the Surma Group are the fluvial Tipam and Dupi Tila Groups, which have been subdivided into three distinct facies (Sincavage et al., 2020; Figure 3). The F1 facies consists of meter-scale beds of fine to medium sandstone with 0.5 m trough cross bedding, interpreted to represent distributary channel deposits on the lower

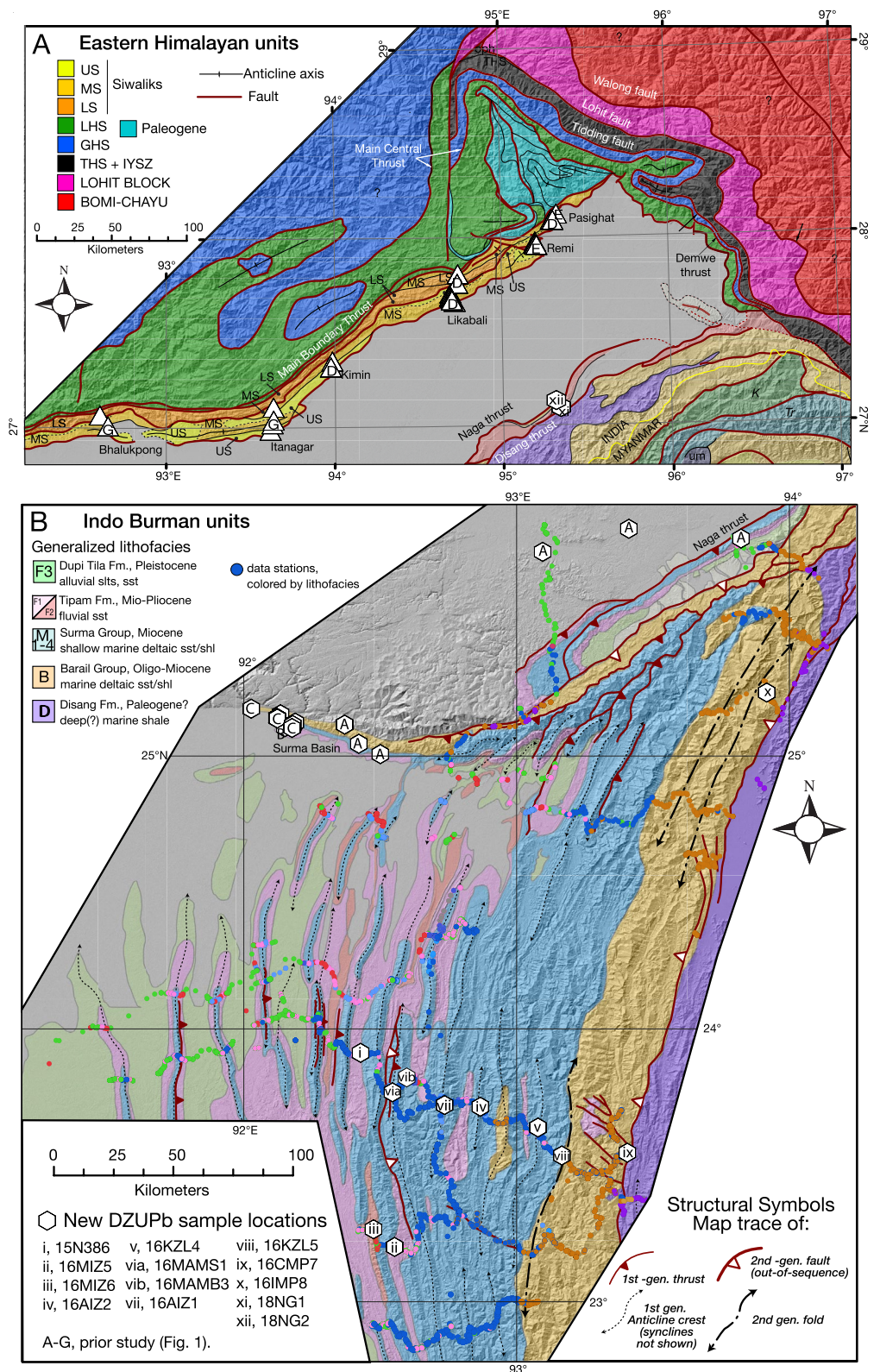**Figure 2.** Geologic maps of the (a) eastern Himalaya and (b) Indo-Burman Ranges. New and published detrital zircon U-Pb basin sample localities are shown after Figure 1. Maps compiled after Acharyya (2007), Agarwal et al. (1991), Betka et al. (2018), Burgess et al. (2012), Haproff et al. (2018), Kumar (1997), Lang et al. (2016), Nandy (1999, 2001), Thura Tun et al. (2014), Yin, Dubey, Kelty, et al. (2010) and new data in this study.
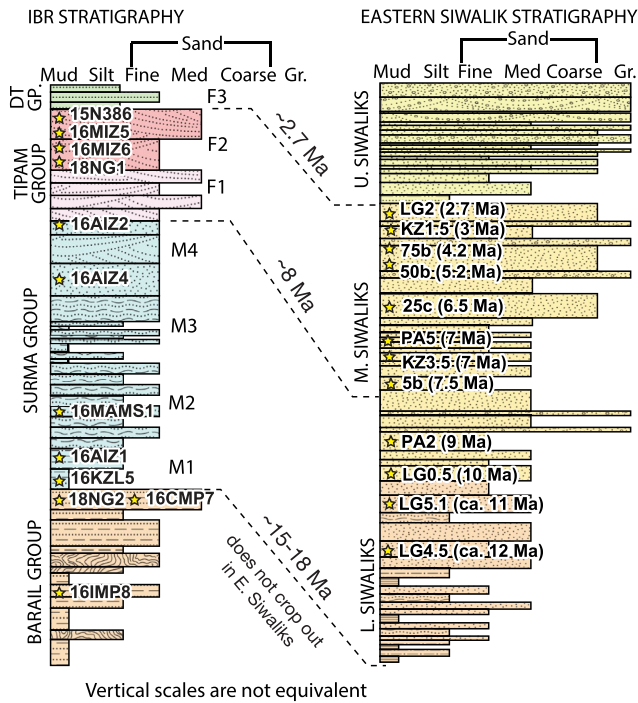
Figure 3. Generalized Miocene-Pliocene stratigraphy of the Indo-Burman Ranges (IBR) and eastern Siwalik foreland basin. IBR stratigraphy includes marine (M1-M4) and fluvial (F1-F3) facies designations of the Surma, Tipam, and Dupi Tila Groups after Sincavage et al. (2020). Eastern Siwalik foreland basin stratigraphy compiled after Chirouze et al. (2012), Lang and Huntington (2014) and Lang et al. (2016). The IBR section represents up to 8 km of stratigraphic thickness, the eastern Siwalik section represents ∼5 km of stratigraphic thickness.

delta plain (Sincavage et al., 2020). The F2 facies contains tan medium sands with thick (tens of meters) beds exhibiting both tabular and trough cross bedding. The scale and character of F1 and F2 deposits are similar to those found on modern cut banks of the Brahmaputra River in Bangladesh, and these deposits are interpreted as channel deposits from the mainstem of the ancestral river (i.e., Tipam Group, Sincavage et al., 2020). The F3 facies resembles the Dupi Tila Group, with thinly bedded (10s of cm) multi-colored silt and fine sand, interpreted as small channels draining local catchments. The Dupi Tila Group overlies the Tipam Group and is widely recognized as locally sourced late-Pliocene to Pleistocene alluvium (Alam et al., 2003).

Magnetostratigraphic analyses from a 1,280 m thick section near the top of the Tipam Group (F2 facies) place it between 4.6 and 3.3 Ma (Lalnuntluanga, 2013), consistent with field observations that document a gradational contact between the Tipam and Surma Groups (Sincavage et al., 2020) and dzFT maximum depositional age estimates of ∼8 Ma (Betka et al., 2018) and ∼7 Ma (Bracciali et al., 2016) near the base of the Tipam Group in the outer belt of the IBR. The fluvial Tipam Group prograded over the shallow marine Surma Group from ∼8 Ma until the avulsion of the braid-belt west of the Shillong Massif between 5 and 3 Ma (Govin, Najman, Copley, et al., 2018; Sincavage et al., 2020).

2.3. Tectonic Setting of the Eastern Himalaya

The eastern Himalaya comprise the India-Eurasia collision zone east of 89°E longitude, including Bhutan, Arunachal Pradesh and southeastern Tibet (Figures 2 and 3). Thrust-bounded tectono-stratigraphic units of Indian crust affinity crop-out continuously along the orogen, forming a semi-continuous crustal wedge (DeCelles et al., 2016; Yin, Dubey, Kelty, et al., 2010). In the eastern Himalaya, the Main Frontal Thrust floors small thrust faults that uplift sedimentary units in the Sub-Himalaya along the foreland basin margin (Agarwal et al., 1991). The Main Boundary Thrust is structurally above Sub-Himalayan units and contains tectonically imbricated Paleozoic and Proterozoic medium to low grade metamorphic rocks of the Lesser Himalayan Series (LHS). The Main Central Thrust overrides LHS units, uplifting crystalline and high-grade metamorphic rocks of the Greater Himalayan Series (GHS; DeCelles et al., 2016; Yin, Dubey, Kelty, et al., 2010; Figure 2). Above the GHS are Paleozoic and Mesozoic sedimentary rocks of the Tethyan Himalayan Series (THS) in the hanging wall of the north-dipping and extensional South Tibetan Fault system. The remnant Tethyan suture zone defines the northern margin of the Indian Plate, where rocks of the Himalayan wedge are in tectonic contact with the late Mesozoic—early Cenozoic Trans-Himalayan Arc plutonic units in the southern Lhasa terrane. The suture zone is primarily a tectonic mélange containing deformed and metamorphosed marine sediments and ophiolitic sequences of the Tethyan ocean basin that closed during the India–Eurasia continental plate collision.

2.4. Eastern Himalayan Siwalik Group Foreland Stratigraphy

The Siwalik Group consists of late Cenozoic sedimentary rocks of the Himalayan foreland basin exhumed along the Main Frontal Thrust in the Sub-Himalayas (e.g., Agarwal et al., 1991; Chirouze et al., 2012, 2013; Cina et al., 2009; Govin, Najman, Copley, et al., 2018, Govin, Najman, Dupont-Nivet, et al., 2018; Lang & Huntington, 2014; Lang et al., 2016; Yin, Dubey, Kelty, et al., 2010). Sedimentary rocks of the eastern Sub-Himalaya are traditionally grouped into three subunits (Jain et al., 1974; Kumar, 1997; Ranga Rao, 1983; Yin, Dubey, Kelty, et al., 2010); while a variety of nomenclatures exist for subunit names, we adopt the Lower, Middle, and Upper Siwalik sub-Group classification consistent with the designation used across the Himalayan foreland (Cerveny et al., 1988; Chirouze et al., 2012; DeCelles et al., 1998; Govin, Najman, Copley, et al., 2018; Govin, Najman, Dupont-Nivet, et al., 2018; Lang et al., 2016; Pilgrim, 1913; White et al., 2002). The Lower Siwalik sub-Group is characterized by interbedded, fluvial-deltaic mudstone and sandstone forming cyclical packages on the order of a

few meters thick (Chirouze et al., 2012; Figure 3). The succession coarsens upwards in the Middle Siwalik from fine to medium and coarse sandstone (Chirouze et al., 2012; Lang et al., 2016). The Middle Siwalik is typified by very thickly bedded medium-coarse "salt and pepper" sandstone that exhibits a wide range of bedforms including climbing ripples, planar bedding and trough cross bedding with ubiquitous coal fragments that reflect deposition by a large, sand-bed river system similar to the modern Brahmaputra River (Chirouze et al., 2012; Govin, Najman, Dupont-Nivet, et al., 2018; Lang et al., 2016). Marine deltaic deposits transition to braided river deposits within the Middle Siwalik along the Dungsam Chu River in Bhutan (Coutand et al., 2016).

The Upper Siwalik is defined by a gradual transition to locally sourced gravel-cobble conglomerate interbedded with sandstone and siltstone (Chirouze et al., 2012; Lang et al., 2016). Debnath et al. (2021) proposed a significant marine incursion between deposition of the Upper and Middle Siwalik sub-Groups based on interpretation of complex bedforms in sandstone and siltstones associated within Upper Siwalik conglomerates. Recent carbon isotope analyses, however, argue against marine incursions of the Himalayan foreland after the Pliocene (Roy et al., 2021). Generally, the Upper Siwalik has been interpreted to reflect Pleistocene foreland progradation of wet alluvial fans fed by transverse river drainages (Burbank, 1992; Lang et al., 2016).

3. Methods

3.1. Geologic Mapping, Lithofacies Characterization, Detrital Zircon Fission-Track (dzFT) and (U-Th)/Pb (dzUPb) Geochronology

A geologic map of the Indo-Burma and Naga fold-thrust belt (Figure 2) was constructed from new observations and prior geologic mapping of the Geologic Survey of India (Nandy, 1999, 2001), Betka et al. (2018), and Sincavage et al. (2020). Because the region is densely vegetated, outcrop lithofacies observations were primarily made at road-cut outcrops along several strike-normal transects across the fold-belt (Figure 2b). Lithofacies were classified using four marine shelfal to intertidal facies (M1-4) for the Miocene Surma Group and three nonmarine fluvial facies (F1–3) for the late Miocene to Pleistocene Tipam and Dupi Tila Groups (Sincavage et al., 2020). Eocene to early Miocene strata of the Barail and Disang Groups (Biswas & Mukhopadhyay, 2011; Johnson & Alam, 1991) were not subdivided. Stratigraphic contacts and regional structures were extrapolated along-strike between geologic traverses using a hillshade map generated from the Shuttle Radar Topography Mission 1 arc second (30 m) digital elevation data (Jet Propulsion Laboratory, NASA). A geologic map of the eastern Himalaya of northern Arunachal Pradesh was compiled from published maps. Map compilation sources are listed in the caption of Figure 2.

New dzFT analyses were performed on five samples to constrain the maximum depositional ages of the Tipam and Barail Groups in the Naga belt (samples 18NG1 and 18NG2, respectively) as well as the Surma (samples 16MAMB3, 16MAMS1) and Barail (sample 16CMP7) Groups in the IBR. Age distributions were analyzed with IsoplotR (Vermeesch, 2018) using the minimum age mixing model of Galbraith (2005) to constrain the maximum depositional age of the deposits (discussed below). Results are presented in Figure 4, alongside previous dzFT results from the Tipam Group (Betka et al., 2018). The dzFT analytical methods are described in Supporting Information S1.

Twelve samples were collected (samples i-xii in Figures 2 and 5) from the IBR units (Tipam, Surma, and Barail Groups) for high-n (~300 grains per sample) dzUPb analysis. Samples were collected to test for spatio-temporal dzUPb provenance trends that span the IBR section from the Barail Group to the Tipam Group. Hand samples were shipped to Zirchron LLC for mineral separation. Large-n dzUPb LA-ICPMS analyses were conducted on zircon separates at the Arizona LaserChron Center (Pullen et al., 2014). Results are presented in Figure 5. Sample locations and new dzUPb results are tabulated in Data Set S1 and Data Set S2 and the dzUPb analytical methodology are provided in Supporting Information S1.

3.2. Quantitative Regional dzUPb Compilations and Stratigraphic Correlations

To test for spatio-temporal provenance trends in IBR dzUPb age distributions, the 12 new datasets (Figure 5) were plotted by stratigraphic group and quantitatively compared with previously published IBR dzUPb results using DZstats, a MATLAB code for statistical comparison of detrital geochronology datasets (Saylor and Sundell, 2016). Cumulative distribution functions (CDFs) are presented in Figure 6 and kernel density estimates
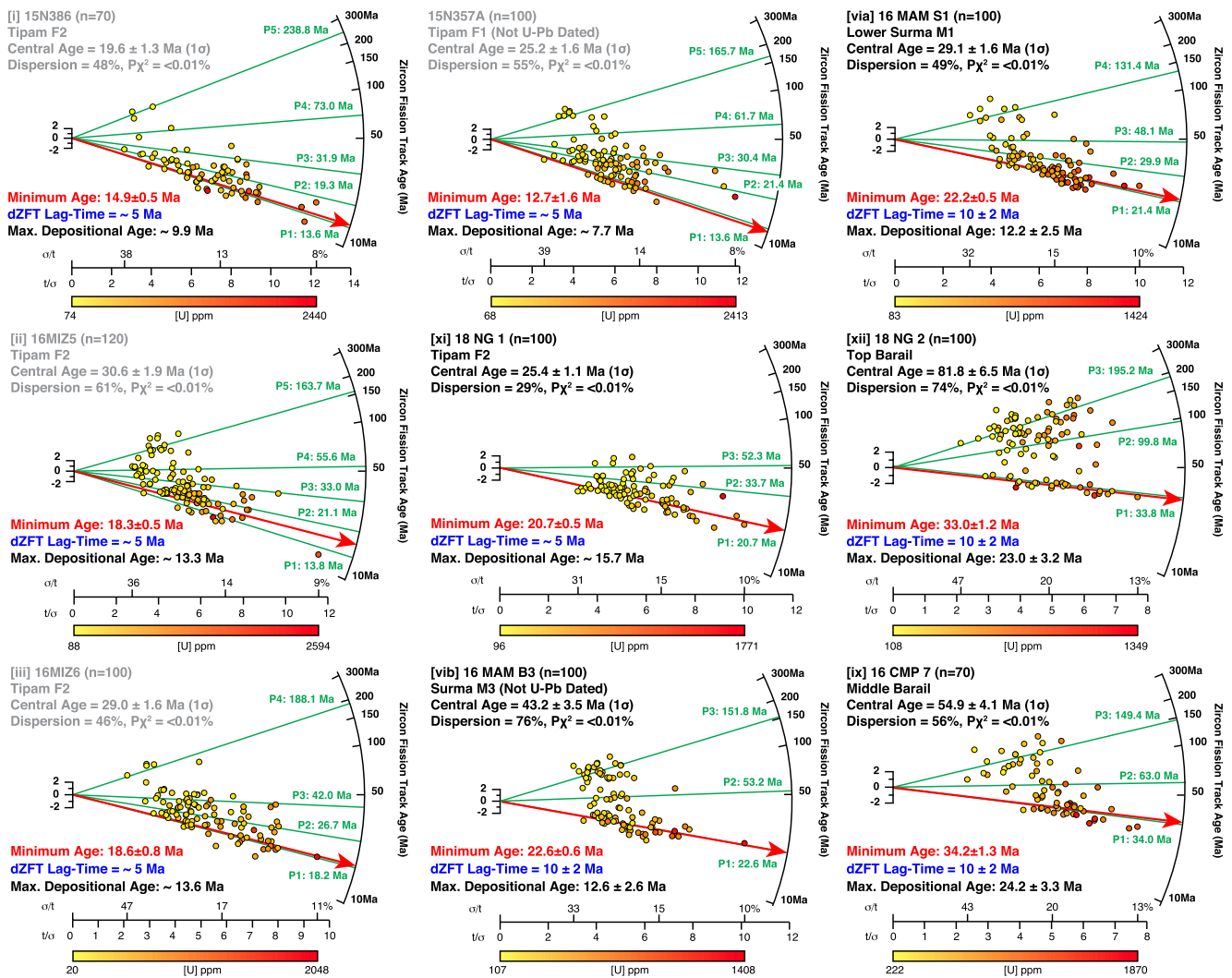
Figure 4. Radial plots showing detrital zircon fission track (dzFT) results from the Indo-Burman Ranges (IBR) and Naga belt, roman numerals correspond with sample locations in Figure 2. Samples are arranged in stratigraphic order down the columns from left to right. The minimum ages (red line) and peak ages (green text and lines) were calculated using IsoplotR (Vermeesch, 2018). Data from Tipam samples (shown with gray text) 15N386, 16MIZ5, 16MIZ6, and 15N357 are from Betka et al. (2018) with minimum and peak ages recalculated using IsoplotR. New IBR dzFT data (samples 16MAMB3, 16MAMS1, and 16CMP7) and Naga belt samples (18NG1 and 18NG2) are indicated with bold type. Maximum depositional ages were determined by subtracting the assigned dzFT lag-time from the IsoplotR minimum age. Full dzFT data tables are available in Data Set S5.

(KDEs) for the basin dzUPb compilations are presented in Supporting Information S2. Intersample statistical results are reported using three statistical tests: the KDE cross-correlation coefficient, the Kuiper V statistic, and the Kolmogorov-Smirnov D statistic (basin compilation data and results are tabulated in Data Set S3 and Data Set S4). In this paper, the KDE cross-correlation coefficient (R^2) of cross-plots between samples is generally favored to evaluate the (dis)similarity of compared age distributions. The diffusion-based adaptive bandwidth (Botev et al., 2010) is uniformly applied as the smoothing parameter to define the KDE for each sample age distribution. The KDE bandwidth provides a useful substitute for analytical error when comparing samples from different labs and when analytical uncertainties are not known for all datasets (Saylor & Sundell, 2016; Sundell and Saylor, 2017). The KDE cross-correlation coefficient is sensitive to the presence or absence of peaks, peak shape and peak size (Saylor & Sundell, 2016). The Kolmogorov-Smirnov Test D statistic (KSD) and Kuiper test V statistic (KV) represent the maximum distance between the empirical CDF of two samples (i.e., lower KSD and KV values indicate a better fit). The KSD and KV statistics do not account for single-grain error or KDE bandwidth, only the empirical age distribution. The KSD is more sensitive to median than tails of distribution while
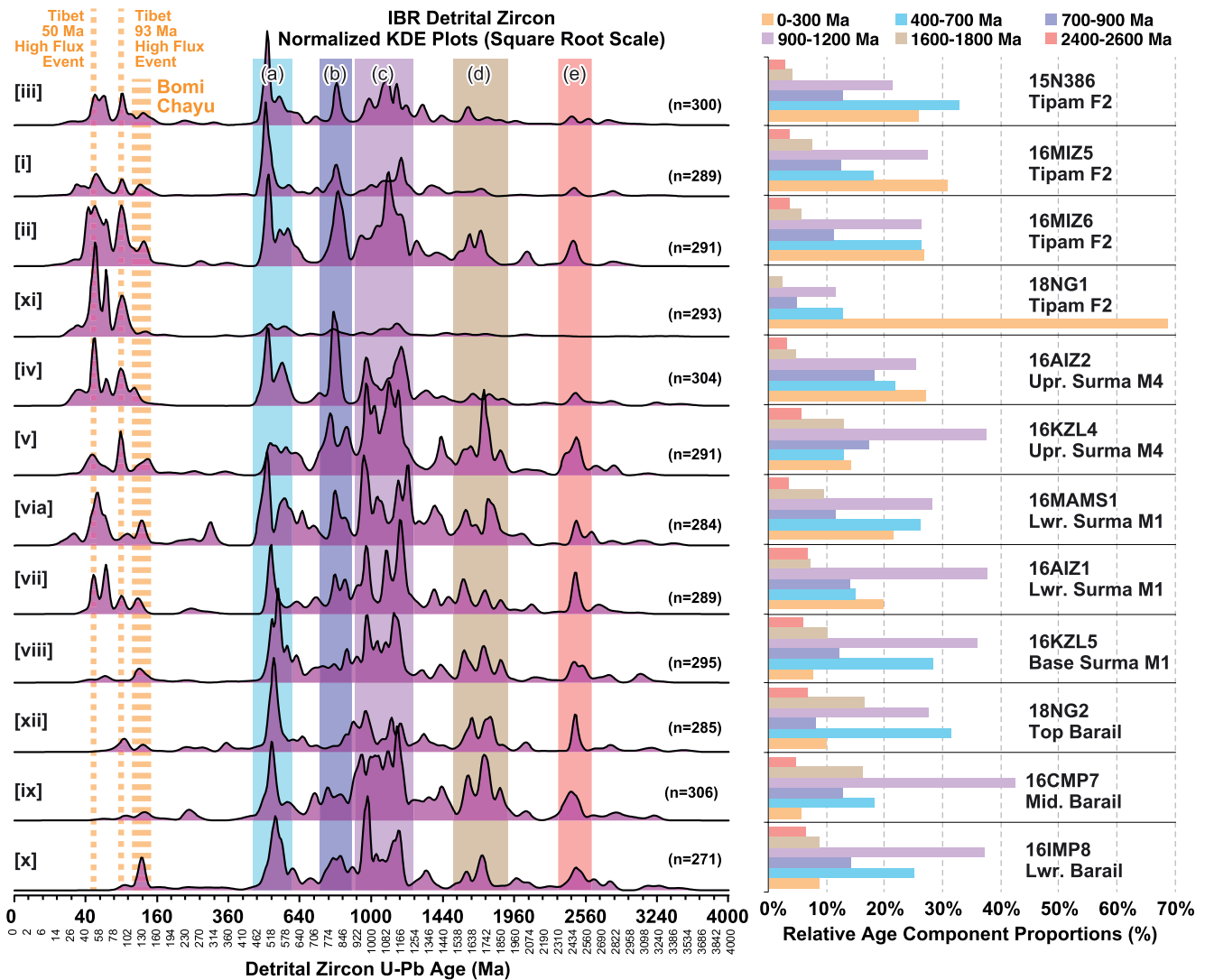
Figure 5. Left, kernel density estimate (KDE) plots of new dzUPb age distributions for 12 samples collected from the Indo-Burman Ranges (IBR) and Naga belt. Samples are arranged in stratigraphic order (youngest on top). Five pre-Mesozoic age populations that are present in most of the samples are highlighted with colored bars (a–e). Three <300 Ma age populations common to the Gangdese and Bomi Chayu batholiths are also indicated; HFE, high-flux event. The horizontal axis is displayed with a square root scale to highlight trends in the <300 Ma part of the distribution. Right, stacked column chart showing the relative proportions of the six dominant age populations present in IBR dzUPb data. Full dzUPb data tables are available in Data Set S2.

the KV is evenly weighted across the distribution. Although the KDE cross-correlation coefficient is favored, consistency between the three statistical tests affirms results.

Basin dzUPb sample sizes of $n > 375$ are required to use the KDE cross-correlation coefficient to consistently discriminate age populations that were derived from the same source from those that were derived from different sources (Saylor & Sundell, 2016). Therefore, individual samples from corresponding stratigraphic intervals with statistically similar age distributions (qualitatively identified from the CDFs) were combined to form high-n (>500) dzUPb compilations for each stratigraphic group (Figures 5–8; Supporting Information S2, Data Set S3, and Data Set S4). Regional dzUPb provenance analyses were compiled from published literature and combined with our new data to create high-n dzUPb datasets for IBR and eastern Himalayan Siwalik units. Individual sample datasets were grouped by basin (either IBR or Siwalik), formation and stratigraphic position, age, spatial proximity, and their dzUPb age distributions. The DZStats intersample compare tool was used to test the viability of combining data from different studies of the same unit to build high-n (>300 grains/sample) datasets. Closely spaced samples of the same formation were grouped first and intraformational
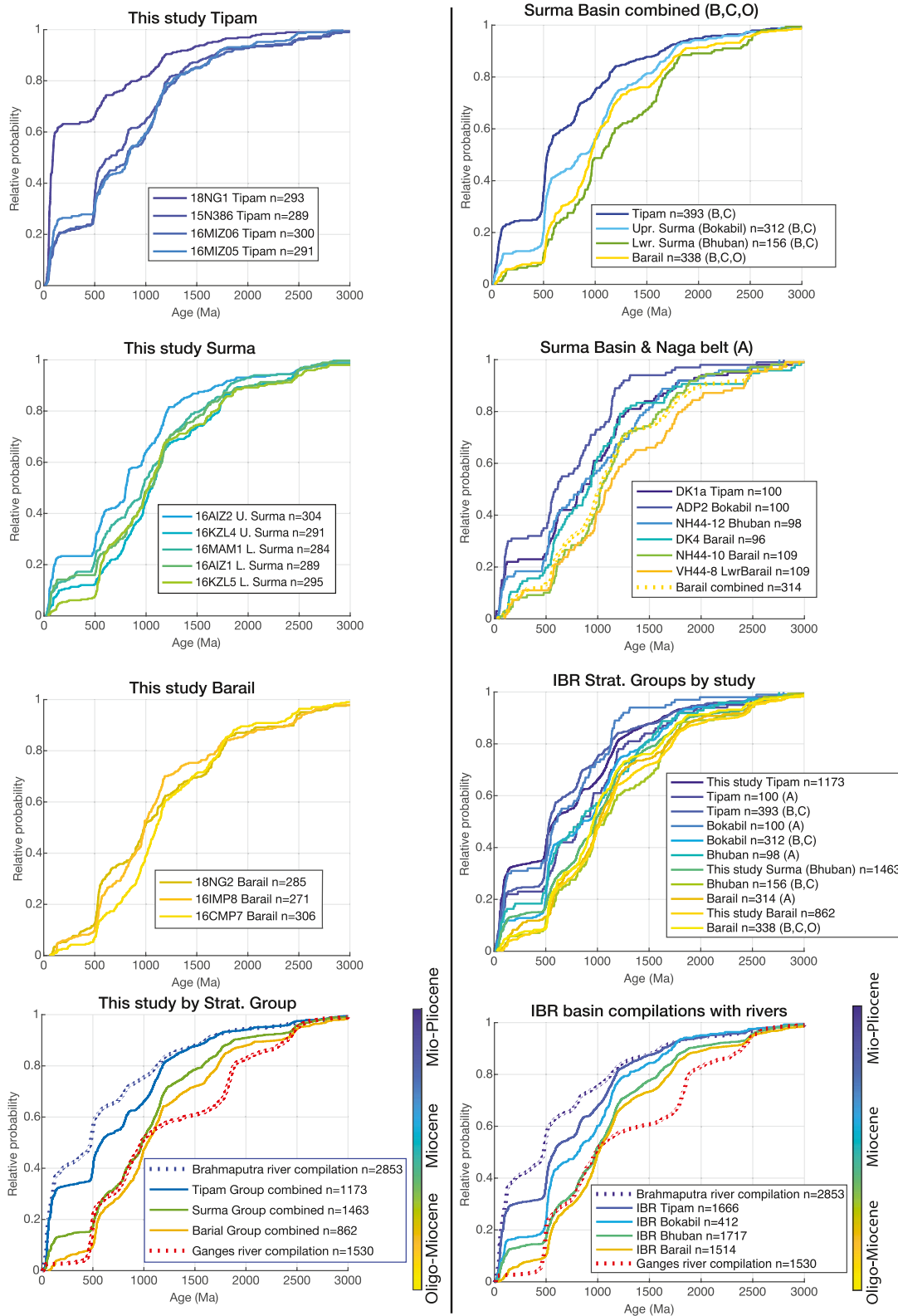
Figure 6.
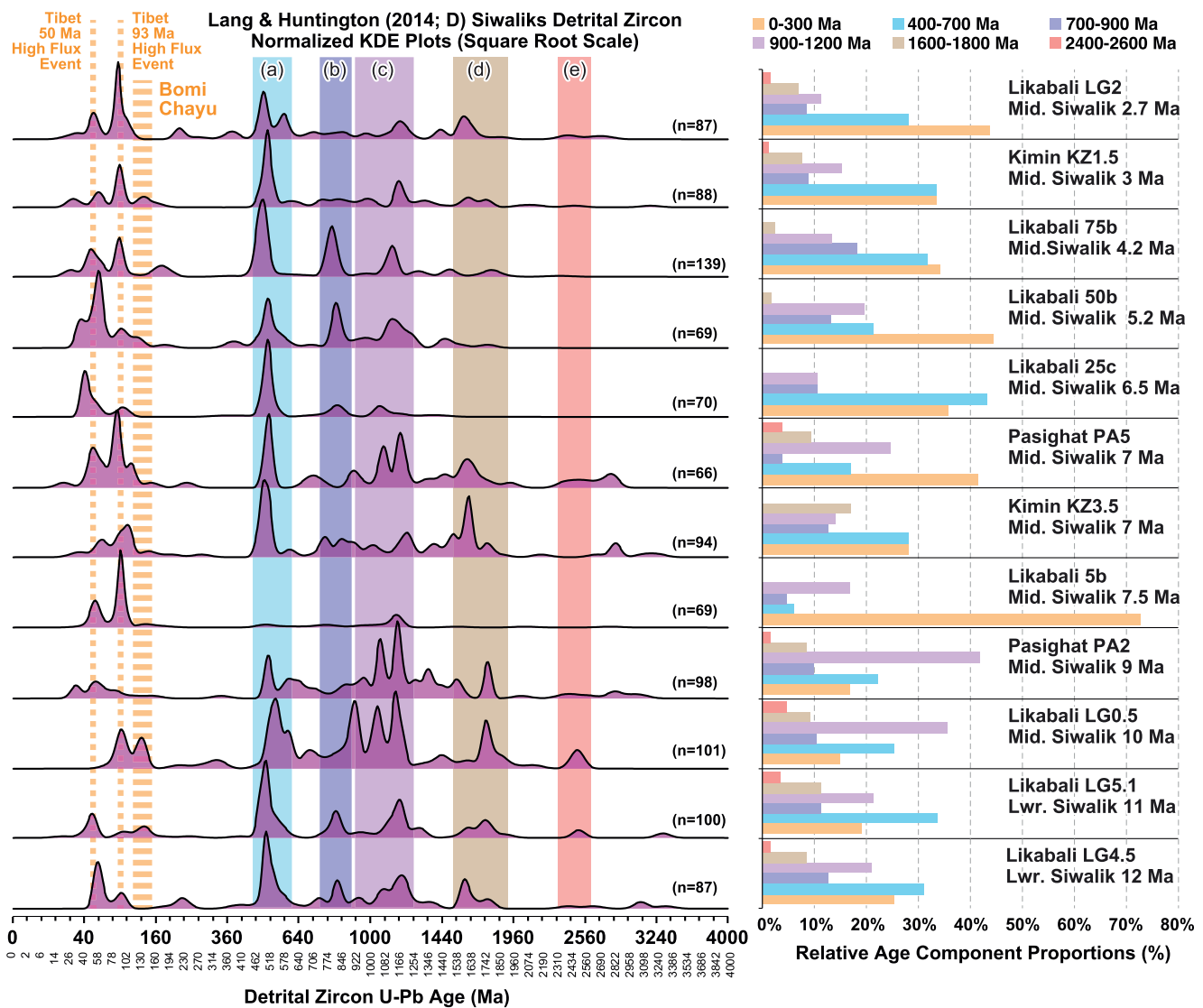
Figure 7. Left, kernel density estimate plots of Siwalik Group dzUPb data from Lang and Huntington, 2014. Samples are arranged by to stratigraphic order and proximity to the Himalaya (youngest and most proximal on top). The horizontal scale and IBR age populations (<300 Ma and a–e) are shown as in Figure 5. Right, stacked column chart showing the relative proportions of the six dominant age populations present in Siwalik Group dzUPb data.

groups were expanded as long as there was a good correlation between the age distributions of the group and the additional sample. In some cases, individual sample n-values were too low ($n < 70$) to yield meaningful intersample statistical results. These low-n samples were grouped with nearby samples of the same formation to increase the site n-value regardless of their statistical correlation. For example, in two studies (Bracciali et al., 2015; Yang et al., 2018) dzUPb samples were collected from the same outcrops in the Surma Basin so they were grouped by formation to increase the n-value for datasets from this location. Basin sample locations are shown in Figures 1 and 2. IBR dzUPb datasets from the Surma Basin and Naga belt (Figure 6) were compiled from Bracciali et al. (2015), Najman et al. (2008), Vadlamani et al. (2015), and Yang et al. (2018). Eastern Himalaya Siwalik Group dzUPb datasets (Figures 7 and 8) were compiled from Cina et al. (2009), Govin,

Figure 6. Left, cumulative distribution function (CDF) plots showing Indo-Burman Ranges (IBR) dzUPb age distributions and IBR compilations by stratigraphic group (bottom left). Right, CDFs of previously published IBR dzUPb age data compiled by stratigraphic group and combined with new data from this study (bottom right). Color scale approximates the stratigraphic age. IBR compilations are plotted with dzUPb age distributions from modern alluvium of the Ganges and Brahmaputra Rivers to highlight provenance trends through time. Letters in parenthesis correspond to the data sources listed in Figure 1. Sample locations are shown in Figures 1 and 2. Bokabil and Bhuban correspond to the upper and lower Surma Group, respectively.
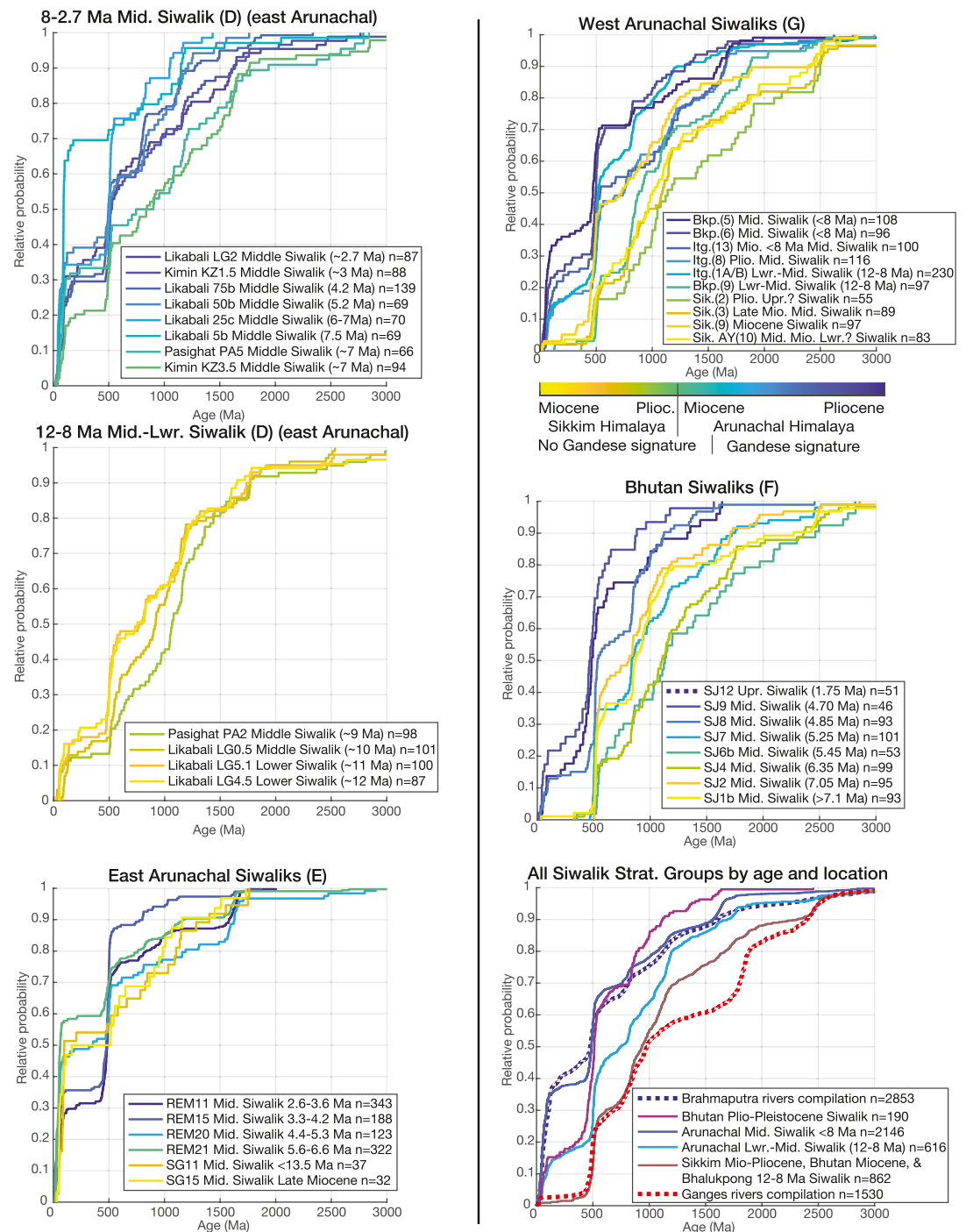
Figure 8. Cumulative distribution function plots showing eastern Himalaya Siwalik Group dzUPb data compiled from prior studies. Letters in parentheses correspond with the data sources and sample locations listed in Figures 1 and 2. Siwalik basin compilations are shown in the bottom right with the modern Ganges and Brahmaputra River compilations. Color scale indicates approximate age as in Figure 6.

Najman, Copley, et al. (2018), Govin, Najman, Dupont-Nivet, et al. (2018), and Lang and Huntington (2014). High-n dzUPb age compilations were then used to quantitatively correlate between IBR and Siwalik deposits of similar age to create regional IBR–Siwalik large-n dzUPb basin compilations (Figure 9; Supporting Information S2, Data Set S3, and Data Set S4).

3.3. Source Compilations and Characterization of Basin dzUPb Provenance Trends

To test for spatio-temporal trends in IBR and Siwalik basin dzUPb data, high-n basin compilations were compared with published dzUPb age compilations from Himalayan bedrock source terranes (sample locations in Figure 1). Bedrock data from the LHS, GHS, and THS + uLHS were compiled by Gehrels et al. (2011). GHS, THS, and uLHS data were grouped to form a single Himalayan hinterland source to contrast with Himalayan foreland (LHS) and Tibetan sources. Lhasa terrane data were compiled from Gehrels et al. (2011), Guo et al. (2017), Hu et al. (2019), Li et al. (2014), Q. Wang et al. (2021), and Zhu et al. (2011). Bedrock zircon age distributions from the Gangdese Arc were taken from the compilations in Lang and Huntington (2014) and Zhu et al. (2017). Bomi Chayu batholith, EHS, and Namche Barwa Massif bedrock zircon age data were compiled from Lang and Huntington (2014).

To contextualize late Cenozoic temporal trends in the IBR and Siwalik basin dzUPb age distributions, dzUPb data were also compiled from modern alluvium of the Ganges and Brahmaputra River systems (sample locations in Figure 1; data compilations in Supporting Information S2 and Data Set S3). Ganges River source data were compiled from the main channel of the modern Ganges (Blum et al., 2018; Campbell et al., 2005) as well as tributaries that drain the frontal part of the Himalayan wedge (Amidon et al., 2005; Bracciali et al., 2015; Cina et al., 2009; Govin, Najman, Dupont-Nivet, et al., 2018). Brahmaputra River source data were compiled from the main braid-belt of the modern Brahmaputra (Bracciali et al., 2015; Cina et al., 2009) as well as tributaries with trans-Himalayan or eastern syntaxis watersheds, including the Yarlung-Tsangpo, Parlung, and Lohit rivers. Although some of the frontal Himalaya rivers in western Arunachal Pradesh, Bhutan, and Nepal currently drain into the modern Brahmaputra River, they are grouped with the Ganges River compilation because they only sample sediment from the Himalayan wedge and, prior to the Pliocene avulsion of the Brahmaputra River north of the Shillong Massif (Govin, Najman, Copley, et al., 2018; Najman et al., 2012), these tributaries probably fed sediment directly to the Bengal Basin, bypassing the Miocene Brahmaputra river.

A dzUPb age unmixing model (DZMix; Sundell and Saylor, 2017) was applied to estimate the relative proportions of Himalayan bedrock and river sources present in the basin dzUPb compilations. DZMix is a MATLAB program for "unmixing" a single detrital geochronology sample using inverse Monte-Carlo modeling to estimate the relative proportions of possible source terranes within a basin sample. The KDEs for each of the input Himalayan source compilations were randomly mixed to find the relative proportion of each source that produced a best fit to the dzUPb age distribution for each basin compilation. Each model was run for 10,000 trials using the scale source distribution function to fit peaks between 0 and 3,500 Ma. The best 1% of solutions were accepted. The model goodness of fit was determined by the KDE cross-correlation coefficient. Model optimization functions and subsampling routines did not significantly improve fits and were not used in these trials. Unmixing model results for individual basin samples and basin compilations are given in Figure 10 and Supporting Information S3. Unmixing models were carried out twice for the IBR samples, first using only bedrock source terranes and again with only the modern river compilations as possible sources (Figure 10).

4. Results

4.1. dzFT Constaints on Maximum Depositional Age

We present dzFT analyses from five new samples (Figure 4 and Data Set S5). In the IBR, dzFT sample 16MAMB3 was collected near the middle of the Surma Group (Bhuban Fm, location vib in Figure 2) and yields a minimum peak age of 22.6 ± 0.6 Ma. Sample 16MAMS1 was collected ~550 m stratigraphically below 16MAMB3 (location "via" in Figure 2) and yields a minimum peak age of 22.2 ± 0.5 Ma (Figure 4). Sample 16CMP7 was collected near the top of the Barail Group (location ix in Figure 2) and has a minimum peak age of 34.2 ± 1.3 Ma. In the Naga belt, samples 18NG1 and 18NG2 were taken from either side of a disconformity separating the Tipam and Barail Group and yield minimum peak ages of 20.7 ± 0.5 Ma and 33.0 ± 1.3 Ma, respectively (locations xi, and xii, in Figure 2). All of datasets have a wide distribution of single grain ages, including a number of older age populations, indicating that none have been thermally reset during burial.

Interpreting true depositional ages from dzFT maximum depositional age results requires consideration of source area zFT lag-times. Prior dzFT data from the Nepalese and eastern Himalayan Siwalik Group (Bernet et al., 2006; Chirouze et al., 2012, 2013; Govin et al., 2020; Jain et al., 2009; Lang et al., 2016) and pre-Siwalik Dumri
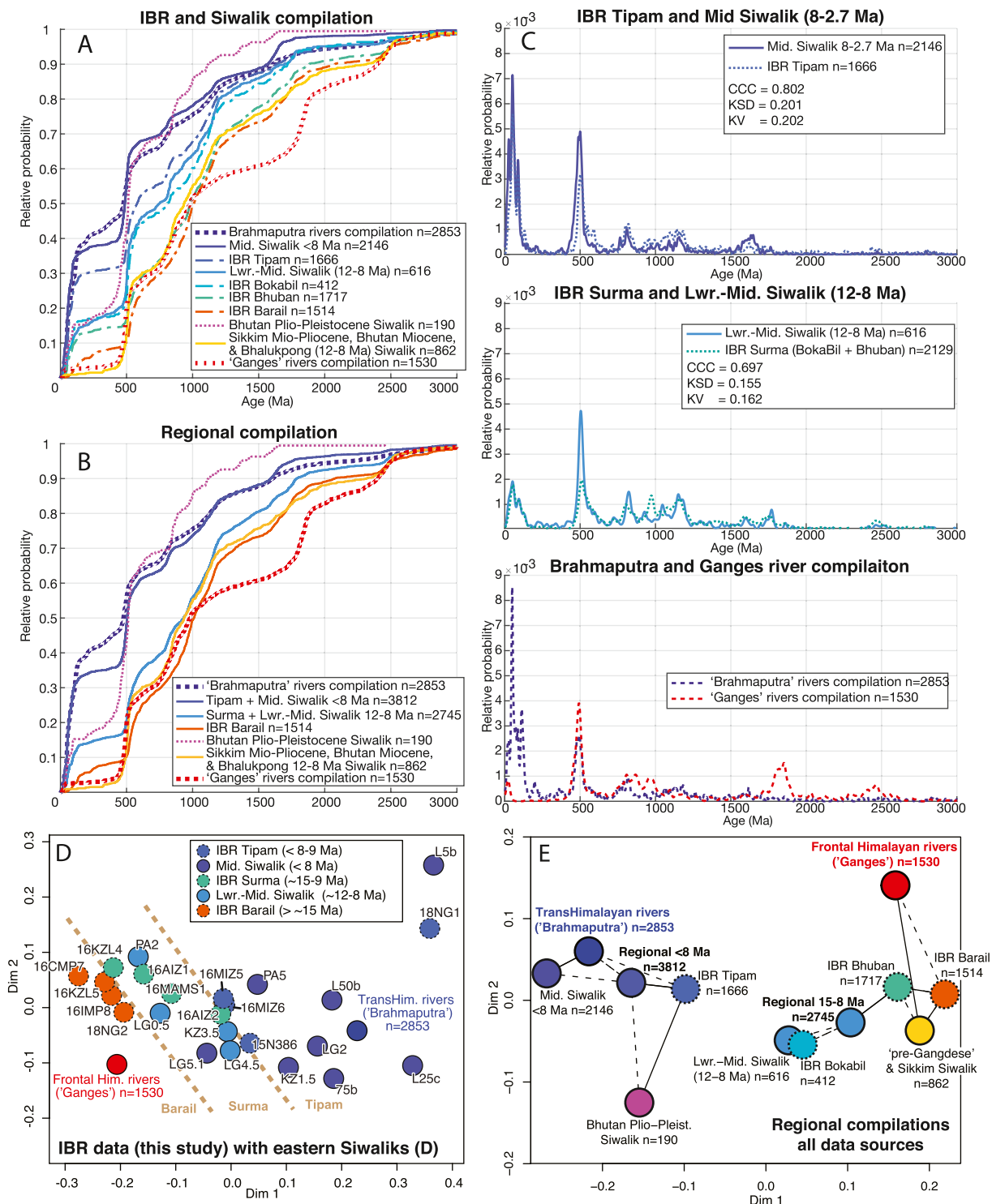
Figure 9. (a) Cumulative distribution function (CDF) plots showing similarity in dzUPb age distributions for equivalent age stratigraphy in the Indo-Burman Ranges (IBR) and eastern Himalaya Siwalik basins. (b) CDFs showing regional compilations of IBR and Siwalik dzUPb data. (c) Kernel density estimate plots with similarity tests between IBR and eastern Himalaya Siwalik dzUPb compilations of equivalent stratigraphic age. The modern Ganges and Brahmaputra River compilations are shown below to highlight provenance trends in the basin data. (d and e) Multi-dimensional scaling plots (KSD statistic) comparing our new data with that of Lang and Huntington (2014) in (d), and the regional dzUPb compilations in (e), highlight dzUPb provenance similarities within IBR-Siwalik deposits and show temporal trends from Ganges-like to Brahmaputra-like provenance up the stratigraphic section. See text for discussion.
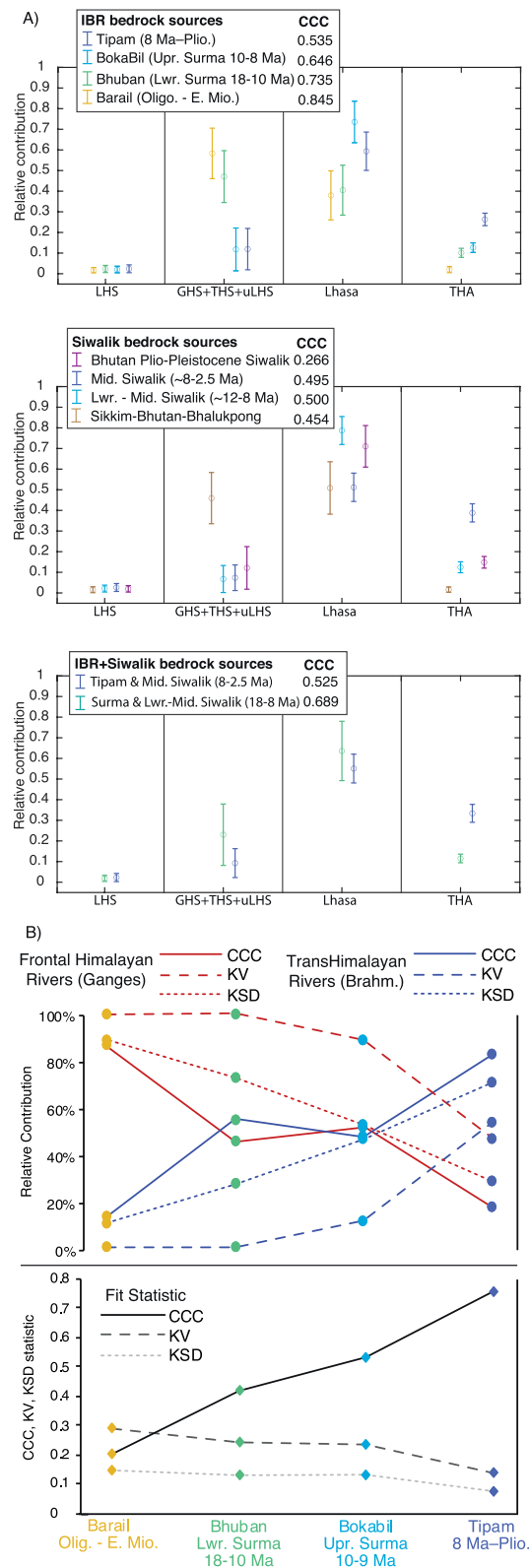
Figure 10.

Formation deposits (Najman et al., 2005; Stickroth et al., 2019) indicate a decrease in zFT lag-times from ~10 Myr, in the early Miocene (i.e., prior to ~16–14 Ma), to a near constant ~5 Myr from the middle Miocene (~12–14 Ma) until the present day. The only exception to this is in latest Miocene to Pleistocene sedimentary deposits sourced from the rapidly exhuming Namche Barwa Massif where dzFT lag-times further decrease from ~5 Myr to as short as ~1–2 Myr after 7–8 Ma, reflecting the onset of rapid exhumation in the Namche Barwa Massif (Govin et al., 2020; Lang et al., 2016; Zeitler et al., 2014). Maximum dzFT depositional age estimates of ~8 Ma were previously reported using minimum single grain ages from four samples of the Tipam Group of the IBR (Betka et al., 2018), including three from samples with new dzUPb results presented here (locations i-iii in Figure 2). However, as noted by Vermeesch (2018), the minimum single grain age, or the youngest age component, can drift to unrealistically young values with increasing sample size. Thus, here we apply the minimum age mixing model of Galbraith (2005) using IsoplotR for the dzFT data from these four samples to ensure convergence on a distinct minimum age estimate independent of sample size (Figure 4). Using an assigned lag-time of ~5 Myr, the youngest minimum age from these four samples of 12.7 ± 1.6 Ma (sample 15N357A, Figure 4) implies a maximum depositional age for the Tipam Group of ~8 Ma, consistent with the previous estimate published in Betka et al. (2018).

Naga belt Tipam sample 18NG1 has a somewhat older minimum age peak of 20.7 ± 0.5 Ma in comparison to the dzFT minimum peak ages of 13–19 Ma from previously dated Tipam samples from the IBR (Betka et al., 2018; Bracciali et al., 2016, Figure 4). The detrital zircon U-Pb ages in this sample indicate a predominantly Tibetan-source (Gangdese Arc, see below). We thus infer that the dzFT lag-time for this sample is longer than that for other Tipam samples given the lower late Cenozoic erosion rates in Tibet upstream from the EHS (e.g., Carrapa et al., 2014, 2017), and that the maximum depositional age for this sample is also ~8 Ma. No very young (<10 Ma) dzFT ages were obtained in any of our Tipam samples in the IBR or Naga belt. Recognizing that such young grains are seen in Siwalik Group rocks younger than ~6.5 Ma (Lang et al., 2016) implies that the Tipam Group of northeast India analyzed in this study is entirely older than 6.5 Ma. However, magnetostratigraphic analysis and dzFT analyses from the top of the Tipam Group indicate that it may be as young as 3–4 Ma where it is exposed in the fold belt farther to the west (Bracciali et al., 2016; Lalnuntluanga, 2013; Najman et al., 2012). Considering that the Tipam Group represents the braid-belt of the ancestral Brahmaputra delta (Johnson and Alam, 1991; Sincavage et al., 2020), we expect the Tipam Group to be systematically younger toward the west as the delta prograded through the late Miocene and Pliocene (Govin, Najman, Copley, et al., 2018). This is consistent with our new data that place the base of the Tipam Group in northeast India at ~8 Ma and previous ages from the top of the formation in the western fold-belt that are ~4 Myr younger.

For the Surma Group, assigning a lag-time of 10 ± 2 Myr for the dzFT minimum peaks ages derived from the middle and lower Surma Group samples 16MAMB3 and 16MAMS1 yields maximum depositional ages of 12.6 ± 2.6 Ma and 12.2 ± 2.5 Ma, respectively. Assigning a shorter lag-time of 7.5 ± 2 Myr, to account for deposition of the Surma Group during the middle Miocene period of time when zFT lag-times decreased, gives a maximum depositional age range of 15.1 ± 2.6 and 14.7 ± 2.5 Ma, respectively. These depositional age ranges match recent estimates based on detrital apatite fission track ages of <17 Ma, and ~9–11 Ma detrital apatite (U-Th)/He ages that are interpreted by Sincavage et al. (2020) as unreset. We thus prefer an ~8 Ma depositional age for the top of the Surma Group. Given the larger uncertainty in early Miocene Himalayan zFT lag times, the age of the base of the Surma Group is less well constrained to between ~15 and 18 Ma. Our results are consistent with magnetostratigraphic data that place depositional age of the middle, and lower, Surma Group at ~12.5–8 Ma, and ~16 Ma, respectively (Lalnuntluanga et al., 2014; Malsawma et al., 2010) and biostratigraphy that places the Bhuban formation of the lower Surma Group firmly in the early Miocene (Tiwari & Kachhara, 2003).

Figure 10. (a) Unmixing results showing the predicted relative contribution and standard deviation of bedrock source terranes modeled for Indo-Burman Ranges (IBR), Siwalik, and IBR + Siwalik basin compilations. Results within each column are arranged by stratigraphic age, younger to the right. Similarity test results (CCC statistic) between input and modeled age distributions are tabulated for each stratal compilation. (b) Unmixing results for IBR data using only the river compilations as possible source terranes. The relative contributions from frontal Himalayan rivers (red curves) and trans-Himalayan rivers (blue curves) are shown (top), as well as the stratigraphic trends in the goodness of fit (CCC, KV, and KSD statistics) for the inversion (bottom). Note that the relative source contributions determined using the river compilations is a mixture of only two possible sources so there is no reported uncertainty in the result.

Biostratigraphy from the Barail Group in the IBR indicate a late Eocene (~38 Ma, Najman et al., 2008; cf. Tiwari and Kachhara, 2003) to early Miocene (Alam et al., 2003; Banerji, 1984; Najman et al., 2008) age for these deposits, before the regional dzFT lag time decreased in the middle Miocene. Assigning a 10 ± 2 Myr lag time, the dzFT minimum peak age for the Upper Barail Group in the IBR (16CMP7) gives a late Oligocene maximum depositional age of 24.2 ± 3.3 Ma. This age matches similar dzFT-derived maximum depositional ages from the Upper Barail Group of the Surma Basin (Najman et al., 2008) and recent magnetostratigraphic age constraints of ~27 to 24 Ma from a ~380 m stratigraphic section near the top of the Barail Group (Lalremruatfela, 2020). The minimum dzFT peak age for Barail Group sample 18NG2 from the Naga belt indicates a similar maximum depositional age of 23.0 ± 3.3 Ma. Notably, there is 5–10 Myr gap in time between the top of the Barail Group and the base of the Surma Group. This contact, although poorly exposed, has been interpreted as transgressive onlap upon an erosion surface (Alam et al., 2003; Banerji, 1984), and thus, the top of the Barail Group may have spanned into the early Miocene before being eroded.

4.2. IBR dzUPb Age Populations and Provenance Trends

Normalized KDEs of our new IBR dzUPb results are shown in Figure 5 (data in Data Set S2). Five pre-Mesozoic age populations are common to most of the samples, indicating shared sediment sources: 400–600 Ma (a), 700–900 Ma (b), 900–1,200 Ma (c), 1,500–1,800 Ma (d), and 2,400–2,600 Ma (e). These IBR KDE age distributions, and the relative proportions of these age components, show two qualitative trends through the stratigraphic section. Although all of the samples contain grains from each of the five age populations, the relative proportion of grains in populations (c), (d) and (e) decreases up-section beginning with the stratigraphic transition between the Surma and Tipam Groups (Sample 16AIZ2). The proportion of populations (a) and (b) show no apparent decrease, but quite wide variability. Second, the KDEs also show a marked increase in the proportion of late Phanerozoic grains (<300 Ma) beginning with the deposition of the Surma Group (Sample 16AIZ1, Figure 5). Late Phanerozoic (<300 Ma) age populations are characteristic of the Gangdese and Bomi Chayu batholiths of the Trans-Himalayan Arc, and show several increases up-section in samples of the Surma and Tipam Groups, as the contributions from older populations (c), (d) and (e) diminish. Plotting the data in cumulative distribution functions (Figure 6) illustrates that the relative proportion of grains <300 Ma is strongly correlated with stratigraphic group. The <300 Ma population generally comprises <10% of dzUPb grains in the Barail Group and the basal Surma sample 16KZL5, ~15%–25% of the grains in the Surma Group, and >25% of the grains in the Tipam Group and the upper Surma Group (Bokabil Fm.) sample 16AIZ2 (Figures 5 and 6). The dzUPb age distributions between individual samples within stratigraphic groups are strongly similar and individual samples were combined to create high-n dzUPb compilations for each group (Figure 6).

To test for regional trends in IBR dzUPb provenance, our new data were compared with published IBR dzUPb datasets from the Surma Basin and Naga Belt (Bracciali et al., 2015; Najman et al., 2008; Vadlamani et al., 2015; Yang et al., 2018). Age distributions from the published data are equivalent to those of our new results for each stratigraphic interval (Figure 6, and Supporting Information S2, Data Set S3, and Data Set S4). No significant spatial trends were revealed, and thus, a regional compilation was made for each stratigraphic interval by combining our new data with the published results. Compared with the modern river compilations, the IBR dzUPb age compilations show a systematic trend up section from frontal-Himalayan "Ganges-like" sources in the Barail Group to a more trans-Himalayan "Brahmaputra-like" source in the Tipam Group. In the next sections, the IBR regional dzUPb compilations are used for quantitative stratigraphic correlations with the eastern Himalaya Siwalik Group and for delineation of Himalayan source terranes that contributed sediment to each stratigraphic group.

4.3. Quantitative Comparison Between IBR Strata and the Eastern Himalaya Siwalik Group

Stratal and spatial trends in the late Phanerozoic (grains <300 Ma) dzUPb population from eastern Himalaya Siwalik Group have been thoroughly described by Cina et al. (2009), Govin, Najman, Copley, et al. (2018), Govin, Najman, Dupont-Nivet, et al. (2018), Govin et al. (2020), Lang and Huntington (2014), and Lang et al. (2016) and are only briefly summarized here to contextualize comparisons with IBR dzUPb compilations. The <300 Ma Trans-Himalayan Arc population is present throughout the Lower, Middle and Upper Siwalik Groups (13.5–2.6 Ma) in the central and eastern part of Arunachal Pradesh (Cina et al., 2009; Govin, Najman, Dupont-Nivet, et al., 2018; Lang & Huntington, 2014). In western Arunachal Pradesh, this population does not appear in the sequence until the Middle Siwalik Group (~8 Ma; Bhalukpong section of Cina et al., 2009 correlated with sec-

tions in Chirouze et al., 2012). The first appearance of the Trans-Himalayan Arc signal is even younger (∼5 Ma) in Bhutan (Govin, Najman, Copley, et al., 2018) and entirely absent from the Siwalik Group in the Sikkim Himalaya to the west (Cina et al., 2009). These spatio-temporal trends have led the prior authors to interpret the westward progradation of Neogene trans-Himalayan sedimentary systems that supplied the Siwalik basin with sediment from Tibet, but never reached westward of the present location of the Brahmaputra River (cf., Chirouze et al., 2013; Govin, Najman, Copley, et al., 2018).

Comparison of temporal trends in Siwalik dzUPb age distributions reveal similar patterns to those in the IBR basin. Siwalik Group strata were subdivided by age according to magnetostratigraphic sections in Chirouze et al. (2012) and Lang et al. (2016) that were correlated along-strike for comparison with age-equivalent deposits of the IBR. Figure 7 shows normalized KDEs of dzUPb data from Siwalik Group strata in eastern Arunachal Pradesh (Lang & Huntington, 2014). Each of the five pre-Mesozoic, and the <300 Ma, age populations are present in Siwalik strata in similar proportions as the age-equivalent IBR Surma and Tipam Groups (Figures 5 and 7). The data from Middle Siwalik strata <8 Ma (Lang & Huntington, 2014) yield dzUPb age distributions with >25% of the population comprising grains <300 Ma. The Lower Siwalik to lower Middle Siwalik (∼12–8 Ma) section yields 15%–25% grains <300 Ma. The dzUPb age distributions for the <8 Ma, and 12–8 Ma Siwalik strata match those from the age-equivalent IBR Tipam and Surma Groups, respectively. These comparisons hold true when data from additional Siwalik studies in the eastern Himalaya are considered. Middle Siwalik (<8 Ma) deposits from the Remi River in eastern Arunachal (Govin, Najman, Dupont-Nivet, et al., 2018) yield >30% of grains <300 Ma. Similarly, the <8 Ma Bhalukpong and Itanagar Siwalik sections of western Arunachal (Cina et al., 2009) contain ≥15% grains <300 Ma. Thus, two large-n dzUPb compilations were created by combining data from 8–2.6 Ma and 12–8 Ma deposits of the eastern Siwalik Group (CDFs in Figure 8; intersample comparison statistics in Data Set S4). Data from Bhutan (Govin, Najman, Copley, et al., 2018), the 12–8 Ma Bhalukpong section, and the Sikkim section (Cina et al., 2009) were grouped separately owing to their younger (Bhutan section), or absent (8–12 Ma Bhalukpong and Sikkim sections), Trans-Himalaya Arc population (discussed above).

Quantitative comparisons between IBR and Siwalik dzUPb compilations are given in Figure 9. The IBR strata record changes from more frontal-Himalayan (Ganges-like) sources to more trans-Himalayan (Brahmaputra-like) sources starting with the deposition of the Surma Group (18-8 Ma), with an additional increase in more Brahmaputra-like sources beginning with the deposition of the Tipam Group (<8 Ma). The central and eastern Arunachal Siwalik Group strata match the IBR trends, dzUPb age distributions from the 12-8 Ma Siwalik sections are nearly identical to those from the Surma Group with a CCC value of 0.7. Likewise, dzUPb age distributions from the 8–2.6 Ma Siwalik Group closely resemble those of the Tipam Group (CCC = 0.8), although multi-dimensional scaling (MDS) plots (Vermeesch, 2013; Figure 9d) show the younger Siwalik Group samples (<8 Ma) trend more towards a Brahmaputra-like dzUPb signal than the Tipam Group samples. These results demonstrate that the early to late Miocene (18-8 Ma) and late Miocene to Pliocene (8–2.6 Ma) IBR and eastern Siwalik sections were part of the same ancestral Brahmaputra sediment-routing system (Figure 9). This result is consistent with the observation that the shallow marine-facies of the Surma Group was deposited in a more distal position than the non-marine and more proximal facies of the Siwalik basin from ∼18-8 Ma (Figures 2 and 3). Moreover, these deposits were prograded by the large ancestral Brahmaputra fluvial system that is represented by the Middle Siwalik and Tipam Groups after ∼8 Ma (Sincavage et al., 2020). The dzUPb provenance results are also consistent with prior work that suggests sediment derived from the Trans-Himalayan Arc had not been deposited in the westernmost Arunachal and Bhutan regions of the Siwalik basin until ∼5 Ma (Govin, Najman, Copley, et al., 2018), altogether constraining the lateral continuity and extent of the Neogene Brahmaputra delta to the eastern Siwalik and Indo-Burman basins (cf., Govin, Najman, Copley, et al., 2018; Najman et al., 2012; Sincavage et al., 2020).

4.4. Delineation of Himalayan Source Terranes and Their Stratigraphic Trends

The IBR and Siwalik stratal compilations provide high-n ($n > 500$) datasets that are useful for quantitative comparison (Saylor & Sundell, 2016; Sundell & Saylor, 2017) with known sediment sources of the ancestral Brahmaputra delta and describe how these source contributions have changed through the late Cenozoic. Prior work has identified both Himalayan and Tibetan sources in IBR (Bracciali et al., 2015; Najman et al., 2008, 2012; Vadlamani et al., 2015) and eastern Siwalik deposits (Cina et al., 2009; Govin, Najman, Copley, et al., 2018; Govin, Najman, Dupont-Nivet, et al., 2018; Lang & Huntington, 2014). Supporting Information S3 contains normalized KDEs showing zircon-UPb age distributions for Himalayan bedrock source terranes (listed in the

Methods section) and the dzUPb compilations for modern alluvium from frontal Himalaya ("Ganges-like") and trans-Himalayan ("Brahmaputra-like") rivers. Qualitative comparison with the basin data (Figures 5–8) demonstrates that all five pre-Mesozoic age populations (a-e) and the late Phanerozoic peaks (grains <300 Ma) present in the basin data match with significant peaks from at least one of the Himalayan source terranes. The observed late Miocene increase in dzUPb grains <300 Ma, and synchronous decrease in populations c, d, and e (Figures 4 and 7) among IBR and Siwalik deposits reflects an influx of Trans-Himalayan Arc-derived sediment to the basin at the expense of contributions from Himalayan-derived sediment (LHS, GHS + THS + uLHS).

Figure 10a presents source terrane unmixing results (DZMix, Sundell and Saylor). Best-fit mixtures of Himalayan and Tibetan bedrock sources can be satisfactorily matched to the basin sample dzUPb age-distributions with CCC values between 0.5 and 0.85 (Figure 10a). Some model runs with lower fit statistics (e.g., CCC <0.5) likely reflect sampling bias in the characterization of the source terranes, as present-day bedrock zircon-UPb source compilations do not perfectly record the Miocene exposure of Himalayan terranes. Similarly, the large error bars for some source contributions reflect ambiguity in the inversion where multiple sources have overlapping age populations. For example, population "a" peaks are prominent in both Lhasa and GHS + THS + uLHS sources and population "c" and "d" peaks are also present in multiple sources (Supporting Information S3). Despite these caveats, the unmixing results reveal some significant and systematic trends in the relative contributions of Himalayan sources to IBR strata (Figure 10a).

Both Lhasa terrane and late Phanerozoic (<300 Ma) grains characteristic of the Trans-Himalayan Arc are present in all of the IBR units. The Trans-Himalayan Arc population is present in small proportions (∼3%) for the Barail Group. No grains of ∼50 Ma, typical of the Gangdese batholith along the Yarlung-Tsangpo suture zone (Chapman & Kapp, 2017), are found until deposition of the Surma Group. The few late Phanerozoic grains in the Barail Group are likely derived from the Bomi Chayu and Lohit batholiths exposed south of the current main Himalayan divide (the Lohit batholith zircon-UPb age peak is ∼90 Ma, Lang & Huntington, 2014). The proportion of the Lhasa terrane dzUPb signal shows an apparent increase from the Barail Group to the Tipam group. However, the Lhasa source must be interpreted with caution and may not be a good indicator of trans-Himalayan drainage for two reasons: (a) its zircon-UPb age distribution has a similar shape to the GHS + THS + uLHS source compilation of the frontal Himalayan terranes, and (b) the Lhasa terrane is the host rock of the Bomi Chayu and Lohit batholiths, and thus it is not a unique trans-Himalayan source in the eastern Himalaya. In contrast, the proportion of Trans-Himalayan Arc sediment shows several increases up section from ∼3% in the Barail Group, increasing to 10%–15% in the Surma Group, and increasing again to ∼30% in the Tipam Group, consistent with our more qualitative assessment of late Phanerozoic zircon grains from the KDE plots (Figure 5). This unequivocal increase in Trans-Himalayan Arc grains is balanced by a decrease in the proportion of GHS + THS + uLHS grains from ∼50% to 60% in the Barail and lower Surma Groups to ∼10% in the upper Surma and Tipam Groups. LHS sources do not contribute significantly to the IBR basin, perhaps because large parts of this terrane may not have been exhumed until the late Miocene or later (DeCelles et al., 2016; Long et al., 2012; Salvi et al., 2021; Yin, Dubey, Kelty, et al., 2010).

Unmixing results from the 12–8 Ma and 8–2.6 Ma eastern Siwalik compilations show similar trends to the IBR models for equivalent-age strata (Figure 10a). The Sikkim–Bhutan–Bhalukpong Siwalik Group deposits to the west, without Trans-Himalayan Arc zircons, are also shown to benchmark the provenance of the Siwalik Group without the Brahmaputra delta. Trans-Himalayan Arc-derived zircon are present in significant proportions in eastern Siwalik compilations, confirming the Miocene to Pliocene westward progradation of the paleo-Brahmaputra delta (Govin, Najman, Copley, et al., 2018; Sincavage et al., 2020).

Combined IBR and Siwalik group unmixing results (Figure 10a) give the regional provenance trends for the early Miocene to Pliocene (18–2.6 Ma) delta. The unmixing results for the three compilations (IBR, Siwalik, and combined) yield equivalent relative contributions and provenance trends from each source terrane for coeval deposits. GHS + THS + uLHS, Lhasa and Trans-Himalayan Arc sources all contributed significant volumes of sediment to the delta with the Trans-Himalayan Arc proportion increasing up stratigraphic section at the expense of the other Himalayan sources, particularly sediment derived from frontal Himalayan terranes (GHS + THS + uLHS).

Unmixing models were also carried out with the IBR data using the modern river compilations as sources (Figure 10b). The results show systematic trends from a frontal Himalayan watershed ("Ganges-like") to a trans-Himalayan watershed ("Brahmaputra-like") up stratigraphic section from the Barail Group to the Tipam Group. The

fit statistics improve as the delta provenance becomes increasingly similar to the modern Brahmaputra watershed. Although the base of the lower Siwalik Group does not crop out in the eastern Himalaya, the arrival of the paleo-Brahmaputra delta is preserved in the stratigraphic record of the IBR. Our dzUPb results demonstrate that the early Miocene stratigraphic transition from the Barail Group to the Surma Group (~18–15 Ma) corresponds to an increase in the proportion of Trans-Himalayan Arc grains at the expense of GHS + THS + uLHS grains, reflecting enhanced erosion and headward expansion of the upper paleo-Brahmaputra watershed into the Tibetan Gangdese portion of the Trans-Himalayan Arc. Both 18–8 Ma and 8–3 Ma IBR and Siwalik deposits share eastern Himalaya and Trans-Himalayan Arc (Tibetan) provenance, respectively, confirming the arrival and progradation of a large (>100,000 km^2) ancestral Brahmaputra delta from the early (~18–15 Ma) to late Miocene (~8 Ma; cf., Sincavage et al., 2020).

5. Discussion

Our new IBR high-n dzUPb results and regional IBR–Siwalik basin compilations allow for quantitative evaluation of both the Miocene to Pliocene evolution of the paleo-Brahmaputra watershed (upstream) as well as downstream sediment routing to the Bengal–Nicobar Fan. The following discussion synthesizes first-order trends in dzUPb provenance throughout this late Cenozoic source-to-sink depositional system.

5.1. Implications for Upstream Evolution of the Paleo-Brahmaputra Watershed

The presence of <300 Ma detrital zircons in all of the IBR and Siwalik strata requires contribution from the Trans-Himalayan Arc. Although a minor component, Trans-Himalayan Arc zircons of the Bomi Chayu and Lohit batholiths are observed in the Barail Group, indicating that a suture-crossing river existed in the Oligocene and delivered a relatively small proportion (~3%) of Trans-Himalayan Arc-derived sediment to the Bengal Basin (cf., Bracciali et al., 2016; Najman et al., 2008). Despite their presence throughout Neogene deposits, the most prominent trend revealed in our dzUPb provenance analyses is the systematic increase in the relative contribution of Trans-Himalayan Arc grains up section from the Barail Group to the Tipam Group that we interpret to reflect expansion and/or reorganization of suture-crossing rivers at the eastern margin of the India-Eurasia collision.

Figure 11a presents CDFs that compare the <300 Ma dzUPb populations from each of the IBR and Siwalik compilations with zircon-UPb age distributions from each of the three major components of the Trans-Himalayan Arc compilation that might have contributed sediment to the upstream part of the ancestral Brahmaputra watershed: the Gangdese batholith, bedrock of the eastern Himalayan and Namche Barwa Massif, and the Bomi Chayu batholiths (Lang & Huntington, 2014; Zhu et al., 2017). Sediment from both the 18–8 Ma (lower-middle Siwalik and Surma Group) and the 8–2.6 Ma (middle Siwalik and Tipam Group) basin compilations fall between the age distributions of the Gangdese Arc and the eastern Himalaya–Namche Barwa Massif. The younger population (8–2.6 Ma) plots slightly closer to the eastern Himalaya–Namche Barwa Massif than the older, indicating more EHS bedrock contribution to the delta by the late Miocene. This result is consistent with the dzUPb age distributions from the younger Siwalik Group samples (<7 Ma) that trend more towards a Brahmaputra-like dzUPb signal than the Tipam Group samples (Figures 9d and 9e), and with prior work documenting rapid exhumation of the Namche Barwa Massif that initiated by ~8–10 Ma and persisted until the present day (Govin et al., 2020; Lang et al., 2016; Zeitler et al., 2014). The EHS presently contributes ~50% of the sediment flux to the modern Brahmaputra River (Stewart et al., 2008).

In contrast, the small fraction of <300 Ma zircon grains in the Barail Group are almost exclusively older than ~60 Ma with peaks typical of the Lohit (~90 Ma) and Bomi Chayu batholiths (~140 Ma) of the easternmost Trans-Himalayan Arc comprising 55% of the distribution (Figure 11a). A ~50 Ma peak diagnostic of the Tibetan Gangdese batholith (Chapman & Kapp, 2017) is not present in our Barail Group samples. Similarly, a population of Trans-Himalayan Arc zircons with ages between ~80 and 300 Ma, consistent with a Bomi Chayu and Lohit batholith-derived source, has been documented in the Eocene upper Yinkiong Group of the eastern syntaxis (Baral et al., 2019), although the depositional age of the Yinkiong Group is debated (Ali et al., 2012; Liebke et al., 2011). These results suggest that the primary source of sediment in rivers draining to the ancestral Bengal Basin changed from a frontal and intra-Himalayan catchment, including the Bomi Chayu and Lohit batholiths, to a more Tibetan catchment, including the Gangdese batholith, beginning with the early to middle Miocene deposition of the Surma Group (Figure 11b).
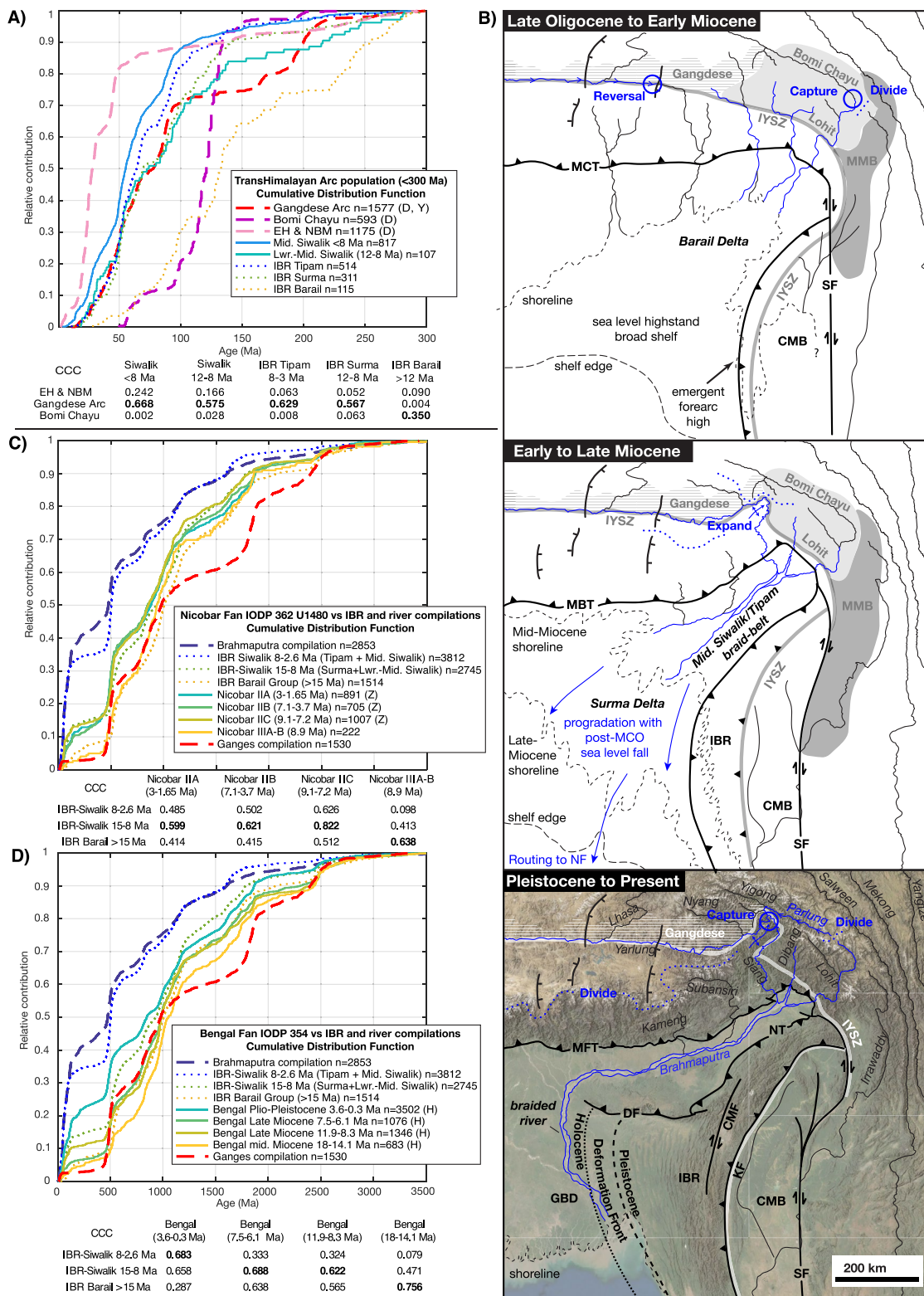
Figure 11.

Integration of the paleo-Yarlung and paleo-Brahmaputra rivers is postulated to have occurred in the early Miocene, predating the onset of rapid exhumation of the Namche Barwa Massif (Figure 11b; Chen et al., 2020; Lang et al., 2016). Our results document a marked increase in the relative proportion of <300 Ma grains, and first appearance of ~50 Ma grains, across the ~18–15 Ma stratigraphic transition from the Barail Group to the Surma Group. This provenance shift records the first definitive expansion of the upper paleo-Brahmaputra watershed into the Gangdese batholith of the Trans-Himalayan Arc and the first arrival of the ancestral Brahmaputra delta to the IBR (cf. Alam et al., 2003; Bracciali et al., 2015; Sincavage et al., 2020).

Leary et al. (2016) propose an early Miocene reversal of the paleo-Yarlung river in response to tectonic uplift in the hanging wall of the Tibetan counter-thrust system and/or geodynamic effects related to roll-back and delamination of the Greater Indian slab (DeCelles et al., 2011). We speculate that the ~20-18 Ma reversal of the paleo-Yarlung river from central to eastern Tibet (Leary et al., 2016), a pulse of incision along the upper Yarlung river ca. 17 Ma (Carrapa et al., 2014, 2017), and 23-15 Ma uplift of the Gangdese batholith (Laskowski et al., 2018) established conditions that were conducive to expansion of the paleo-Brahmaputra river into the paleo-Yarlung watershed from ~18 to 15 Ma. Recent observations of ~15 Ma (Gangdese) Trans-Himalayan Arc zircons in the oldest sampled Miocene sediments of the Bengal Fan (~18-15 Ma, sample 25 in Blum et al., 2018), and geochemical provenance evidence suggesting the presence of Trans-Himalayan Arc sediments in the Nicobar Fan as early as 19 Ma (Chen et al., 2020), are further consistent with this interpretation. The systematic increase of Trans-Himalayan Arc sediment with the IBR-Siwalik deposits from ~18 to 8 Ma, at the expense of GHS + THS + uTHS sediment, records increased erosion of the Trans-Himalayan Arc and expansion of the ancestral Brahmaputra watershed into Tibet through the Miocene (Figure 11b). Below, we propose that regionally more rapid denudation of Tibet during tectonic uplift and monsoon intensification after the middle Miocene Climate Optimum contributed to late Miocene Brahmaputra watershed expansion.

5.2. Downstream Comparison With the Bengal and Nicobar Fans

The new IBR–Siwalik dzUPb compilations complement recent analyses of sediment deposition patterns on the Bengal and Nicobar Fans. In 2015, IODP expedition 354 drilled a 7-site transect of the Bengal Fan that pierced up to 1,080 m of Pleistocene to early Miocene sediment (France-Lanord et al., 2016). Twenty-five sandstone samples were recovered from the core for high-n (an average of 266 grains/sample) dzUPb geochronology (Blum et al., 2018). In 2016, IODP expedition 362 drilled 1,250 m (site U1480) of late Miocene (~9 Ma) to Pleistocene (0.2 Ma) sediments of the Nicobar Fan (McNeill et al., 2017; Pickering, Carter, et al., 2020; Pickering, Pouderoux, et al., 2020). Twenty sandstone samples were extracted from the core for dzUPb geochronology with an average of 121 grains/sample. Here (Figures 11c and 11d) we compare the new IBR dzUPb compilations with Bengal and Nicobar Fan data to constrain patterns of late Cenozoic trans-Himalayan sediment routing through the Bengal Basin. In general, all of the Miocene to Pliocene sediment in the Bengal and Nicobar fans record mixing of Ganges and Brahmaputra watersheds (Blum et al., 2018; Pickering, Carter, et al., 2020). The comparisons made here simply quantify first order trends in the similarity, and thus contribution, to Bengal–Nicobar Fan sediment that was routed through the IBR from the eastern Himalaya and Tibet.

Figure 11. (a) Cumulative distribution function (CDF) plots showing stratal trends in the <300 Ma population from basin dzUPb compilations compared with the three major components of the Trans-Himalayan Arc: the Gangdese batholith, Bomi Chayu batholith, and eastern Himalayan and Namche Barwa bedrock. (b) Interpreted eastern Himalaya drainage reorganization and delta evolution since the Oligocene. Deltaic deposits of the Oligocene Barail Group are fed primarily by frontal Himalayan rivers with limited drainage across the suture zone to the Bomi-Chayu and Lohit batholiths. Only ~5% of the sediment supply is sourced from the Bomi-Chayu and Lohit batholiths. Increased Trans-Himalayan Arc contributions to the Surma Group (18–8 Ma), and the first appearance of the ~50 Ma Gangdese batholith population, record significant expansion of the Brahmaputra River into the Yarlung River watershed. The Surma Group and Lower Siwalik units record intertidal, deltaic, and upper shelf depositional environments. The Middle Siwalik and Tipam Groups (8–2.7 Ma) record fluvial deposition in a sand-bed braided river system that prograded the Surma–Lower Siwalik delta by ~8 Ma. Increased contribution of Trans-Himalayan Arc zircons up section records tectonic uplift and denudation of the Namche Barwa Massif and Gangdese batholith. Southward progradation of the fluvial system during late Miocene sea level fall aids sediment routing over the shelf edge to the Nicobar Fan by 9 Ma. By the Pleistocene, the Brahmaputra River had avulsed to its present course north and west of the Shillong Massif (e.g., Govin, Najman, Copley, et al., 2018; Najman et al., 2012). Blue colored rivers indicate interpreted primary drainages. Abbreviations: IYSZ, Indus-Yarlung Suture Zone; MMB, Mogok Metamorphic Belt; CMB, Central Myanmar Basin; SF, Sagaing Fault; MCT, Main Central Thrust; MBT, Main Boundary Thrust; MFT, Main Frontal Thrust; CMF, Churachandpur-Mao Fault; KF, Kabaw Fault; DF, Dauki Fault; NT, Naga Thrust; IBR, Indo-Burma Ranges; NF, Nicobar Fan; MCO, Miocene Climate Optimum; GBD, Ganges–Brahmaputra Delta. (c and d) CDFs showing comparisons between IBR–Siwalik dzUPb compilations with dzUPb compilations from equivalent age deposits in the Nicobar (c) and Bengal (d) Fan. The CCC intersample statistics are tabulated to quantify comparisons between the stratal compilations. Letters in parentheses correspond with data sources in Figure 1 and: Y, Zhu et al. (2017); Z, Pickering, Carter, et al. (2020).

5.2.1. Nicobar Fan

Terrigenous sediment input to the Nicobar Fan began at 22.5 Ma, initially consisting of pelagic and hemipelagic deposits with low (0.5 g cm^{-2} kyr^{-1}) mass accumulation rates (Pickering, Pouderoux, et al., 2020). Muddy turbidite deposition dominated until ~10 Ma, when an increase in both mass accumulation rate and sand content are noted. A sharp ~15-fold increase in mass accumulation rate from 3 g cm^{-2} kyr^{-1} to 43 g cm^{-2} kyr^{-1} occurred at ~9 Ma and rapid (>25 g cm^{-2} kyr^{-1}) deposition persisted until 5 Ma (McNeill et al., 2017; Pickering, Pouderoux, et al., 2020). The ~9 Ma increase in Nicobar Fan mass accumulation rate is synchronous with shifts in trace element and isotopic (ε_{Nd} and $^{87}Sr/^{86}Sr$) geochemistry that is interpreted to represent rapid exhumation of the EHS (Chen et al., 2020). The large change in Nicobar Fan facies, composition, and mass accumulation rate at ~9 Ma is attributed to trans-Himalayan sediment routed from the IBR (McNeill et al., 2017; Pickering, Carter, et al., 2020; Pickering, Pouderoux, et al., 2020).

Figure 11c compares dzUPb compilations from Nicobar Fan sections IIA, IIB, and IIC with our new IBR-Siwalik compilations. The dzUPb provenance in Nicobar sections IIA (3–1.65), IIB (7.1–3.7 Ma), and IIC (9.1–7.2 Ma) are nearly identical to each other (CCC = 0.81–0.95) and most similar to the IBR 18-8 Ma Surma and lower-middle Siwalik strata (CCC = 0.6–0.8; Figure 11c). In contrast, the older Nicobar section IIIA-B (≥8.9 Ma) lacks a significant proportion of Trans-Himalayan Arc zircons and more closely resembles Barail sediment (CCC = 0.64). These comparisons demonstrate that the ~9 Ma increase in Nicobar Fan mass accumulation rate and shift towards trans-Himalayan-dominated sediment provenance closely resembles the provenance trends which occurred across the stratigraphic transition between the Barail and Surma Groups in the more proximal IBR-Siwalik basin ~6–9 Myr earlier. The limited amount of trans-Himalayan sediment in the Nicobar Fan prior to ~9 Ma suggests that trans-Himalayan sediment delivered to the IBR was initially stored on the shelf, accumulating the shallow-marine to intertidal deposits of the Surma Group and terrestrial deposits of the lower to middle Siwaliks, or routed west of the Ninetyeast Ridge to the Bengal Fan (Pickering, Carter, et al., 2020). We thus infer that the ~9 Ma sharp increase in Nicobar Fan mass accumulation rate reflects the late Miocene progradation of the fluvial part (Tipam Group) of the ancestral Brahmaputra delta over the shallow marine section (Surma Group), routing sediment over the shelf edge and primarily to the Nicobar Fan.

5.2.2. Bengal Fan

The Bengal Fan received sediments from both the Brahmaputra Delta and the Ganges Delta prior to their merger following the westward avulsion of the Brahmaputra River between 5 and 3 Ma (Govin, Najman, Copley, et al., 2018; Sincavage et al., 2020). The Bengal Fan mass accumulation rate increased twice in the middle-to-late Miocene; first from 2 to 15 g cm^{-2} kyr^{-1} at 13.5 Ma, and again from 15 to 25 g cm^{-2} kyr^{-1} over the interval from 11 to 9 Ma. The Bengal Fan mass accumulation rate then decreased to 10 g cm^{-2} kyr^{-1} by 8 Ma (Pickering, Pouderoux, et al., 2020). To evaluate the (dis)similarity between IBR and Bengal Fan sediment, we subdivide the Bengal Fan dzUPb data into one Plio–Pleistocene group and three Miocene groups that match the age intervals of the Miocene IBR units (<8 Ma, 12–8 Ma, and >14 Ma; Figure 11d). As expected, the Plio–Pleistocene population is most similar to the IBR Tipam–Middle Siwalik and Brahmaputra River compilations (CCC ~0.68, 0.67, respectively), confirming that trans-Himalayan (<300 Ma) sediment flux to the Bengal Fan increased after the 5–3 Ma avulsion of the Brahmaputra River to its present course west of the Shillong Massif (Allen et al., 2008; Blum et al., 2018; Pickering, Carter, et al., 2020; Pickering, Pouderoux, et al., 2020; Robinson et al., 2014).

The middle and late Miocene (8.3–11.9 Ma and 6.1–7.5 Ma) Bengal Fan populations are most similar to the IBR 18–8 Ma Surma Group (CCC = 0.6–0.7; Figure 11d) and the first increase in Bengal Fan mass accumulation rate at 13.5 Ma corresponds, in both time and provenance, with the middle Surma Group. Thus, we deduce that trans-Himalayan sediment was both stored on the shelf in the Surma Group and routed to the Bengal Fan between 13.5 and 9 Ma (see above). The second increase in mass accumulation rate (~11–9 Ma) generally coincides with the progradation of the fluvial Tipam Group in the IBR and the much larger (15-fold) mass accumulation rate spike in the Nicobar Fan. Interestingly, the older late Miocene population (8.3–11.9 Ma) has a slightly higher proportion (10%) of Trans-Himalayan Arc sediment than the younger late Miocene population (5%; 6.1–7.5 Ma) which is consistent with more efficient sediment routing from the Brahmaputra Delta to the Nicobar Fan beginning at 9 Ma (Pickering, Carter, et al., 2020), while the Ganges Delta primarily fed the Bengal Fan. The early Miocene (14.1–18 Ma) Bengal Fan dzUPb age distribution most closely resembles that of the Barail Group (CCC = 0.76) and Nicobar Fan section IIIA-B (≥8.9 Ma; CCC = 0.57), recording sedimentation prior to the onset of significant sediment delivery from the ancestral Brahmaputra River.

5.3. Climate and Tectonic Forcing

Examination of the Bengal Basin sedimentary archives in recent years has yielded detailed insights into allogenic and autogenic controls on the transfer and storage of detritus through the Ganges–Brahmaputra delta–fan system across spatial and temporal scales (Alam et al., 2003; Bergmann et al., 2020; Blum et al., 2018; Bracciali et al., 2015; Goodbred et al., 2014; Govin, Najman, Copley, et al., 2018; Govin, Najman, Dupont-Nivet, et al., 2018; Lang & Huntington, 2014; Pickering, Carter, et al., 2020; Pickering et al., 2014; Sincavage et al., 2018, 2020). Above (Section 5.1), we postulate that ∼18–15 Ma integration of the ancestral Brahmaputra and Yarlung watersheds occurred within or shortly after early Miocene (∼20–17 Ma) tectonic uplift and subsequent reversal of the paleo-Yarlung river (Carrapa et al., 2014; DeCelles et al., 2011; Leary et al., 2016), delivering the first Trans-Himalayan Arc sediment to the Bengal Basin (Bracciali et al., 2015). This period of time also corresponds with uplift along the MCT and exhumation of the Himalayan hinterland (DeCelles et al., 2016; White et al., 2002). At least two later phases of intensified erosion of the eastern Himalaya are documented in the stratigraphic record (Govin et al., 2020). Onset of rapid exhumation in the EHS through coupled tectonic-erosive processes has been proposed as early as 10 Ma (Palin et al., 2015; Zeitler et al., 2014) and accelerated after 8 Ma (Govin et al., 2020). Short zFT and rutile U-Pb lag times (∼1 Myr) determined from Pleistocene deposits of the Bengal–Nicobar fan indicate a later pulse of rapid denudation of the EHS (Najman et al., 2019). Below, we discuss Miocene climate events that were contemporaneous with episodes of coupled tectonic uplift and accelerated denudation of the orogen and likely affected patterns of sediment supply to the Bengal Basin.

Stratigraphic evidence from carbonate sequences in the Maldives of the eastern Indian Ocean identify sea level highstand conditions associated with the Miocene Climate Optimum persisting until ∼15 Ma (Betzler et al., 2018). This would favor sequestration of IBR and Siwalik trans-Himalayan sediments on the shelf in the shallow marine deposits of the Barail and Surma Groups during and shortly after this period of sea-level highstand. The early to late Miocene (∼18-8 Ma) increase in Trans-Himalayan Arc provenance through the Surma and Tipam Groups is also contemporaneous with the initiation of an oxygen minimum zone and enhanced upwelling in the western Indian Ocean and Arabian Sea (Bialik et al., 2020), which gradually expanded eastward towards the Maldives and Ninetyeast Ridge in the Bengal Basin (Betzler et al., 2016). Cooling after the Miocene Climate Optimum initiated expansion of the Antarctic ice sheet (Zachos et al., 2001), which is recognized in the Maldives carbonates as a shift from aggradation to progradation (Betzler et al., 2018) and eventual deposition of drift deposits associated with the onset of monsoon conditions in southeast Asia (Betzler et al., 2016; Bialik et al., 2020). The introduction of cold water from the Southern Ocean during expansion of Antarctic ice volume shifted precipitation bands farther north as sea-level dropped after the Miocene Climate Optimum (Holbourn et al., 2010; Miller et al., 2005; Yang et al., 2020; Zachos et al., 2001) and initiation of the South Asian Monsoon (Betzler et al., 2016) intensified erosion of the high Himalaya (cf. Bretschneider, Hathorne, Bolton, et al., 2021; Bretschneider, Hathorne, Huang, et al., 2021). The timing of these late Miocene eustatic and climatic shifts overlaps with the progradation of the fluvial Tipam Group (∼10-8 Ma) across the paleo-shelf (Sincavage et al., 2020) and an increase in both the mass accumulation rate and proportion of Trans-Himalayan Arc sediment in the Nicobar Fan at ∼9 Ma (Chen et al., 2020; Pickering, Pouderoux, et al., 2020; Pickering, Carter, et al., 2020).

We propose that intensification of monsoon conditions and sea level drop after the Miocene Climate Optimum enhanced erosion in the Himalaya and led to late Miocene progradation of the paleo-Brahmaputra delta and increased sediment delivery to the Bengal and Nicobar Fans. Increased erosion of trans-Himalayan sources was further enhanced by early to late Miocene tectonic uplift in the hinterland of the Himalaya (Carrapa et al., 2014; DeCelles et al., 2016; Laskowski et al., 2017; McQuarrie et al., 2019; White et al., 2002). Late Miocene progradation of the Ganges and Brahmaputra deltas (Lindsay et al., 1991; Najman et al., 2008) filled in the remnant ocean basin between India and the IBR, further increasing sediment transport to the Bengal–Nicobar Fan. The subsequent Pliocene decrease in Nicobar Fan sedimentation rate and following Pleistocene increase in Bengal Fan sedimentation rate has been attributed to a combination of several tectonic and processes including, impingement of the Ninetyeast Ridge on the Sunda Trench (McNeill et al., 2017), the avulsion of the Brahmaputra River around the rising Shillong Massif, and the westward propagation of the Indo-Burman Ranges fold-thrust belt (Betka et al., 2018; Govin, Najman, Copley, et al., 2018; Sincavage et al., 2020).

6. Conclusions and Future Work

The dzUPb age distributions from the 18–8 Ma IBR Surma Group are nearly identical to those from 12–8 Ma Siwalik sections (CCC = 0.7). Likewise, dzUPb age distributions from the <8 Ma IBR Tipam Group are nearly identical to those of the 8–2.6 Ma Siwalik Group (CCC = 0.8). Thus, the late Miocene (18–8 Ma and 8–2.6 Ma) IBR and eastern Siwalik sections can be considered laterally continuous stratigraphic successions with equivalent provenance. The eastern Siwalik Group displays more proximal facies assemblages than the more distal time and provenance equivalent IBR deposits, documenting the existence of an early to late Miocene delta with equivalent size as the modern Ganges–Brahmaputra Delta.

The late Eocene to early Miocene Barail Group dzUPb age distributions lack any significant proportion of Trans-Himalayan Arc grains (<10%) and are dissimilar from younger Miocene IBR and Siwalik deposits. The Barail Group dzUPb provenance indicates denudation of a mostly frontal Himalayan watershed ("Ganges-like"), recording sedimentation prior to the arrival of the ancestral Brahmaputra delta. However, the small proportion of zircon grains in the Barail Group derived from the Trans-Himalayan Arc match zircon-UPb ages of the Lohit and Bomi-Chayu batholiths, indicating that a suture-crossing river delivered sediment to the IBR from the easternmost Trans-Himalayan Arc during the Oligocene, but the watershed had not yet expanded to include the Gangdese batholith in southeastern Tibet.

Provenance trends show systematic patterns from the early to late Miocene in the IBR and Siwalik stratigraphic sections. Contributions from Himalayan sources generally decrease (GHS + THS + uLHS ~60%–10%) up stratigraphic section as Trans-Himalayan Arc sediment increases (~3%–30%). Trans-Himalayan Arc zircon grains in the Surma and Tipam Groups are primarily derived from the Tibetan Gangdese batholith. The first appearance of ~50 Ma Gangdese batholith grains in the IBR section occurs in the lower Surma Group. Trans-Himalayan Arc contributions from eastern Himalaya and Namche Barwa bedrock sources are greater in the younger and more proximal deposits of the Tipam and Middle Siwalik Groups. Together these provenance trends record the increasing integration of the ancestral Brahmaputra and Yarlung drainages from ~18–8 Ma, followed by more rapid denudation of the EHS after 8 Ma.

Late Miocene progradation of the fluvial delta (Tipam Group) delivered sediment over the shelf edge to the Nicobar Fan by 9 Ma and probably reflects sea level fall after the Miocene Climate Optimum. Prior to 9 Ma, trans-Himalayan sediment was both deposited on the shelf in the Surma Group and delivered to the Bengal Fan since at least 18 Ma. We propose that intensification of the South Asian Monsoon after the Miocene Climate Optimum accelerated Himalayan erosion rates, leading to the early to middle Miocene expansion of the ancestral Brahmaputra River into the Tibetan parts of the Trans-Himalayan Arc (Gangdese batholith). The resultant increasing sediment flux drove late Miocene progradation of the paleo-Brahmaputra delta and partially filled the Bengal Basin.

New results presented herein, synthesized with over a decade of previous research in the IBR and Siwalik basins, delineate the Miocene arrival and subsequent progradation of the ancestral Brahmaputra delta in the Bengal Basin. Future chronostratigraphic analyses of the Barail, Surma and Tipam Groups, including high resolution magnetostratigraphy, micropaleontology, and paleoclimate proxy studies, are needed to more precisely associate the timing of major changes in sediment provenance and mass accumulation rates with the proposed Miocene climate and tectonic allogenic forcing events. Regardless of these current limitations, the rich stratigraphic archive of the Indo-Burman Ranges preserves a nearly continuous and understudied record of late Cenozoic climate-tectonic interactions in the eastern Himalaya.

Conflict of Interest

The authors declare no conflicts of interest relevant to this study.

Data Availability Statement

All data needed to evaluate the conclusions in the paper are present in the paper and/or Supporting Information. Supplementary materials are available in the figshare data repository: https://doi.org/10.6084/m9.figshare.16869177.

References

Acharyya, S. K. (2007). Collisional emplacement history of the Naga-Andaman ophiolites and the position of the eastern Indian suture. *Journal of Asian Earth Sciences*, *29*(2–3), 229–242. https://doi.org/10.1016/j.jseaes.2006.03.003

Agarwal, R. P., Srivastava, A. K., & Maithani, A. (1991). Geology of the eastern Himalayan Foothill belt of Bhutan and Arunachal Pradesh: An overview. *Himalayan Geology*, *2*(2), 197–205.

Alam, M., Mustafa Alam, M., Curray, J. R., Lutfar Rahman Chowdhury, M., & Royhan Gani, M. (2003). An overview of the sedimentary geology of the Bengal Basin in relation to the regional tectonic framework and basin-fill history. *Sedimentary Geology*, *155*(3–4), 179–208. https://doi.org/10.1016/s0037-0738(02)00180-x

Ali, J. R., Aitchison, J. C., Chik, S. Y. S., Baxter, A. T., & Bryan, S. E. (2012). Paleomagnetic data support Early Permian age for the Abor Volcanics in the lower Siang Valley, NE India: Significance for Gondwana-related break-up models. *Journal of Asian Earth Sciences*, *50*, 105–115. https://doi.org/10.1016/j.jseaes.2012.01.007

Allen, R., Najman, Y., Carter, A., Barfod, D., Bickle, M. J., Chapman, H. J., et al. (2008). Provenance of the Tertiary sedimentary rocks of the Indo-Burman Ranges, Burma (Myanmar): Burman arc or Himalayan-derived? *Journal of the Geological Society*, *165*(6), 1045–1057. https://doi.org/10.1144/0016-76492007-143

Amidon, W. H., Burbank, D. W., & Gehrels, G. E. (2005). Construction of detrital mineral populations: Insights from mixing of U–Pb zircon ages in Himalayan rivers. *Basin Research*, *17*(4), 463–485. https://doi.org/10.1111/j.1365-2117.2005.00279.x

Banerjee, P., Bürgmann, R., Nagarajan, B., & Apel, E. (2008). Intraplate deformation of the Indian subcontinent. *Geophysical Research Letters*, *35*(18), 1–5. https://doi.org/10.1029/2008gl035468

Banerji, R. K. (1984). Post-eocene biofacies, palaeoenvironments and palaeogeography of the Bengal Basin, India. *Palaeogeography, Palaeoclimatology, Palaeoecology*, *45*(1), 49–73. https://doi.org/10.1016/0031-0182(84)90109-3

Baral, U., Lin, D., Goswami, T. K., Sarma, M., Qasim, M., & Bezbaruah, D. (2019). Detrital zircon U–Pb geochronology of a Cenozoic foreland basin in Northeast India: Implications for zircon provenance during the collision of the Indian and Asian plates. *Terra Nova*, *31*(1), 18–27. https://doi.org/10.1111/ter.12364

Beaumont, C. (1981). Foreland basins. *Geophysical Journal International*, *65*(2), 291–329. https://doi.org/10.1111/j.1365-246x.1981.tb02715.x

Bergmann, F., Schwenk, T., Spiess, V., & France-Lanord, C. (2020). Middle to late Pleistocene architecture and stratigraphy of the lower Bengal fan—Integrating multichannel seismic data and IODP expedition 354 results. *Geochemistry, Geophysics, Geosystems*, *21*(1), e2019GC008702. https://doi.org/10.1029/2019gc008702

Bernet, M., van der Beek, P., Pik, R., Huyghe, P., Mugnier, J.-L., Labrin, E., & Szulc, A. (2006). Miocene to recent exhumation of the central Himalaya determined from combined detrital zircon fission-track and U/Pb analysis of Siwalik sediments, western Nepal. *Basin Research*, *18*(4), 393–412. https://doi.org/10.1111/j.1365-2117.2006.00303.x

Betka, P. M., Seeber, L., Thomson, S. N., Steckler, M. S., Sincavage, R., & Zoramthara, C. (2018). Slip-partitioning above a shallow, weak décollement beneath the Indo-Burman accretionary prism. *Earth and Planetary Science Letters*, *503*, 17–28. https://doi.org/10.1016/j.epsl.2018.09.003

Betzler, C., Eberli, G. P., Kroon, D., Wright, J. D., Swart, P. K., Nath, B. N., et al. (2016). The abrupt onset of the modern South Asian Monsoon winds. *Scientific Reports*, *6*, 29838. https://doi.org/10.1038/srep29838

Betzler, C., Eberli, G. P., Lüdmann, T., Reolid, J., Kroon, D., Reijmer, J. J. G., et al. (2018). Refinement of Miocene sea level and monsoon events from the sedimentary archive of the Maldives (Indian Ocean). *Progress in Earth and Planetary Science*, *5*(1), 1–18. https://doi.org/10.1186/s40645-018-0165-x

Bezbaruah, D., & Muzamil, S. (2013). Deposition history of coal bearing Tikak Parbat Formation of Barail Group in a part of the belt of Schuppen, Northeast India. *South East Asian Journal of Sedimentary Basin Research*, *1*, 50–66.

Bialik, O. M., Auer, G., Ogawa, N. O., Kroon, D., Waldmann, N. D., & Ohkouchi, N. (2020). Monsoons, upwelling, and the deoxygenation of the northwestern Indian Ocean in response to middle to late Miocene global climatic shifts. *Paleoceanography and Paleoclimatology*, *35*, e2019PA003762. https://doi.org/10.1029/2019PA003762

Biswas, A., & Mukhopadhyay, B. P. (2011). Signature of a paleogene submarine-fan from the Jenam Formation, Barail Group, Assam-Arakan orogen, northeastern India. *Journal of the Geological Society of India*, *78*(6), 510–522. https://doi.org/10.1007/s12594-011-0125-1

Blum, M., Rogers, K., Gleason, J., Najman, Y., Cruz, J., & Fox, L. (2018). Allogenic and autogenic signals in the stratigraphic record of the deep-sea Bengal Fan. *Scientific Reports*, *8*(1), 7973. https://doi.org/10.1038/s41598-018-25819-5

Botev, Z. I., Grotowski, J. F., & Kroese, D. P. (2010). Kernel density estimation via diffusion. *Annals of Statistics*, *38*(5), 2916–2957. https://doi.org/10.1214/10-aos799

Bracciali, L., Najman, Y., Parrish, R. R., Akhter, S. H., & Millar, I. (2015). The Brahmaputra tale of tectonics and erosion: Early Miocene river capture in the eastern Himalaya. *Earth and Planetary Science Letters*, *415*, 25–37. https://doi.org/10.1016/j.epsl.2015.01.022

Bracciali, L., Parrish, R. R., Najman, Y., Smye, A., Carter, A., & Wijbrans, J. R. (2016). Plio-Pleistocene exhumation of the eastern Himalayan syntaxis and its domal "pop-up". *Earth-Science Reviews*, *160*, 350–385. https://doi.org/10.1016/j.earscirev.2016.07.010

Bretschneider, L., Hathorne, E. C., Bolton, C. T., Gebregiorgis, D., Giosan, L., Gray, E., et al. (2021). Enhanced late Miocene chemical weathering and altered precipitation patterns in the watersheds of the bay of Bengal recorded by detrital clay radiogenic isotopes. *Paleoceanography and Paleoclimatology*, *36*(9). https://doi.org/10.1029/2021pa004252

Bretschneider, L., Hathorne, E. C., Huang, H., Lübbers, J., Kochhann, K. G. D., Holbourn, A., et al. (2021). Provenance and weathering of clays delivered to the bay of Bengal during the middle Miocene: Linkages to tectonics and monsoonal climate. *Paleoceanography and Paleoclimatology*, *36*(2). https://doi.org/10.1029/2020pa003917

Burbank, D. W. (1992). Causes of recent Himalayan uplift deduced from deposited patterns in the Ganges basin. *Nature*, *357*(6380), 680–683. https://doi.org/10.1038/357680a0

Burgess, P. W., Yin, A., Dubey, C. S., Shen, Z.-K., & Kelty, T. K. (2012). Holocene shortening across the Main Frontal Thrust zone in the eastern Himalaya. *Earth and Planetary Science Letters*, *357–358*, 152–167. https://doi.org/10.1016/j.epsl.2012.09.040

Campbell, I. H., Reiners, P. W., Allen, C. M., Nicolescu, S., & Upadhyay, R. (2005). He–Pb double dating of detrital zircons from the Ganges and Indus Rivers: Implication for quantifying sediment recycling and provenance studies. *Earth and Planetary Science Letters*, *237*(3), 402–432. https://doi.org/10.1016/j.epsl.2005.06.043

Carrapa, B., Hassim, M. F. B., Kapp, P. A., DeCelles, P. G., & Gehrels, G. (2017). Tectonic and erosional history of southern Tibet recorded by detrital chronological signatures along the Yarlung River drainage. *GSA Bulletin*, *129*(5–6), 570–581. https://doi.org/10.1130/b31587.1

Carrapa, B., Orme, D. A., DeCelles, P. G., Kapp, P., Cosca, M. A., & Waldrip, R. (2014). Miocene burial and exhumation of the India-Asia collision zone in southern Tibet: Response to slab dynamics and erosion. *Geology*, *42*(5), 443–446. https://doi.org/10.1130/g35350.1

Cerveny, P. F., Naeser, N. D., Zeitler, P. K., Naeser, C. W., & Johnson, N. M. (1988). History of uplift and relief of the Himalaya during the past 18 million years: Evidence from fission-track ages of detrital zircons from sandstones of the Siwalik Group. In K. L. Kleinspehn, & C. Paola (Eds.), *New perspectives in basin analysis* (pp. 43–61). Springer. https://doi.org/10.1007/978-1-4612-3788-4_3

Chapman, J. B., & Kapp, P. (2017). Tibetan magmatism database. *Geochemistry, Geophysics, Geosystems*, *18*(11), 4229–4234. https://doi.org/10.1002/2017gc007217

Chen, W.-H., Yan, Y., Clift, P. D., Carter, A., Huang, C.-Y., Pickering, K. T., et al. (2020). Drainage evolution and exhumation history of the eastern Himalaya: Insights from the Nicobar Fan, northeastern Indian Ocean. *Earth and Planetary Science Letters*, *548*, 116472. https://doi.org/10.1016/j.epsl.2020.116472

Chirouze, F., Dupont-Nivet, G., Huyghe, P., van der Beek, P., Chakraborti, T., Bernet, M., & Erens, V. (2012). Magnetostratigraphy of the Neogene Siwalik Group in the far eastern Himalaya: Kameng section, Arunachal Pradesh, India. *Journal of Asian Earth Sciences*, *44*, 117–135. https://doi.org/10.1016/j.jseaes.2011.05.016

Chirouze, F., Huyghe, P., Beek, P. V. D., Chauvel, C., Chakraborty, T., Dupont-nivet, G., & Bernet, M. (2013). Tectonics, exhumation, and drainage evolution of the eastern Himalaya since 13 Ma from detrital geochemistry and thermochronology, Kameng River section, Arunachal Pradesh. *GSA Bulletin*, *125*(3–4), 523–538. https://doi.org/10.1130/B30697.1

Cina, S. E., Yin, A., Grove, M., Dubey, C. S., Shukla, D. P., Lovera, O. M., et al. (2009). Gangdese arc detritus within the eastern Himalayan Neogene foreland basin: Implications for the Neogene evolution of the Yalu–Brahmaputra River system. *Earth and Planetary Science Letters*, *285*(1), 150–162. https://doi.org/10.1016/j.epsl.2009.06.005

Clark, M. K., & Bilham, R. (2008). Miocene rise of the Shillong Plateau and the beginning of the end for the Eastern Himalaya. *Earth and Planetary Science Letters*, *269*(3), 337–351. https://doi.org/10.1016/j.epsl.2008.01.045

Clift, P. D., & Jonell, T. N. (2021). Himalayan-Tibetan erosion is not the cause of Neogene global cooling. *Geophysical Research Letters*, *48*(8), e2020GL087742. https://doi.org/10.1029/2020gl087742

Coutand, I., Barrier, L., Govin, G., Grujic, D., Hoorn, C., Dupont-Nivet, G., & Najman, Y. (2016). Late Miocene-Pleistocene evolution of India-Eurasia convergence partitioning between the Bhutan Himalaya and the Shillong Plateau: New evidences from foreland basin deposits along the Dungsam Chu section, eastern Bhutan: Convergence Partitioning East Himalaya. *Tectonics*, *35*, 2963–2994. https://doi.org/10.1002/2016tc004258

Curray, J. R. (1991). Possible greenschist metamorphism at the base of a 22-km sedimentary section, Bay of Bengal. *Geology*, *19*(11), 1097–1100. https://doi.org/10.1130/0091-7613(1991)019<1097:pgmatb>2.3.co;2

Curray, J. R., Emmel, F. J., & Moore, D. G. (2002). The Bengal Fan: Morphology, geometry, stratigraphy, history and processes. *Marine and Petroleum Geology*, *19*(10), 1191–1223. https://doi.org/10.1016/s0264-8172(03)00035-7

Curray, J. R., & Moore, D. G. (1971). Growth of the Bengal deep-sea fan and denudation in the Himalayas. *GSA Bulletin*, *82*(3), 563–572. https://doi.org/10.1130/0016-7606(1971)82[563:gotbdf]2.0.co;2

Debnath, A., Taral, S., Mullick, S., & Chakraborty, T. (2021). The Neogene Siwalik succession of the Arunachal Himalaya: A revised lithostratigrphic classification and its implications for the regional paleogeography. *Journal of the Geological Society of India*, *97*(4), 339–350. https://doi.org/10.1007/s12594-021-1692-4

DeCelles, P. G., Carrapa, B., Gehrels, G. E., Chakraborty, T., & Ghosh, P. (2016). Along-strike continuity of structure, stratigraphy, and kinematic history in the Himalayan thrust belt: The view from Northeastern India: Eastern Himalayan thrust belt. *Tectonics*, *35*(12), 2995–3027. https://doi.org/10.1002/2016tc004298

DeCelles, P. G., Gehrels, G. E., Quade, J., Ojha, T. P., Kapp, P. A., & Upreti, B. N. (1998). Neogene foreland basin deposits, erosional unroofing, and the kinematic history of the Himalayan fold-thrust belt, western Nepal. *GSA Bulletin*, *110*(1), 2–21. https://doi.org/10.1130/0016-7606(1998)110<0002:nfbdeu>2.3.co;2

DeCelles, P. G., Kapp, P., Quade, J., & Gehrels, G. E. (2011). Oligocene–Miocene Kailas basin, southwestern Tibet: Record of postcollisional upper-plate extension in the Indus-Yarlung suture zone. *GSA Bulletin*, *123*(7–8), 1337–1362. https://doi.org/10.1130/b30258.1

Evans, P. (1932). Tertiary succession in Assam. *Transactions of the Mining and Geological Institute of India*, *27*(3), 155–260.

France-Lanord, C., Spiess, V., Klaus, A., & Schwenk, T., & Expedition 354 Scientists. (2016). In *Proceedings of the International Ocean Discovery Program* (Vol. 354). https://doi.org/10.14379/iodp.proc.354.101.2016

Galbraith, R. F. (2005). *Statistics for fission track analysis*. Chapman & Hall/CRC.

Gani, M. R., & Alam, M. M. (1999). Trench-slope controlled deep-sea clastics in the exposed lower Surma Group in the southeastern fold belt of the Bengal Basin, Bangladesh. *Sedimentary Geology*, *127*(3), 221–236. https://doi.org/10.1016/s0037-0738(99)00050-0

Garzanti, E. (2019). The Himalayan Foreland Basin from collision onset to the present: A sedimentary–petrology perspective. *Geological Society, London, Special Publications*, *483*(1), 65–122. https://doi.org/10.1144/sp483.17

Gehrels, G., Kapp, P., Decelles, P., Pullen, A., Blakey, R., Weislogel, A., et al. (2011). Detrital zircon geochronology of pre-Tertiary strata in the Tibetan-Himalayan orogen. *Tectonics*, *30*(5), TC5016. https://doi.org/10.1029/2011TC002868

Goodbred, S. L., Paolo, P. M., Ullah, M. S., Pate, R. D., Khan, S. R., Kuehl, S. A., et al. (2014). Piecing together the Ganges-Brahmaputra-Meghna River delta: Use of sediment provenance to reconstruct the history and interaction of multiple fluvial systems during Holocene delta evolution. *GSA Bulletin*, *126*(11–12), 1495–1510. https://doi.org/10.1130/b30965.1

Govin, G., Najman, Y., Copley, A., Millar, I., van der Beek, P., Huyghe, P., et al. (2018). Timing and mechanism of the rise of the Shillong Plateau in the Himalayan foreland. *Geology*, *46*(3), 279–282. https://doi.org/10.1130/g39864.1

Govin, G., Najman, Y., Dupont-Nivet, G., Millar, I., van der Beek, P., Huyghe, P., et al. (2018). The tectonics and paleo-drainage of the easternmost Himalaya (Arunachal Pradesh, India) recorded in the Siwalik rocks of the foreland basin. *American Journal of Science*, *318*(7), 764–798. https://doi.org/10.2475/07.2018.02

Govin, G., van der Beek, P., Najman, Y., Millar, I., Gemignani, L., Huyghe, P., et al. (2020). Early onset and late acceleration of rapid exhumation in the Namche Barwa syntaxis, eastern Himalaya. *Geology*, *48*(12), 1139–1143. https://doi.org/10.1130/g47720.1

Graham, S. A., Dickinson, W. R., & Ingersoll, R. V. (1975). Himalayan-Bengal model for flysch dispersal in the Appalachian-Ouachita system. *Bulletin of the Geological Society of America*, *86*(3), 273–286. https://doi.org/10.1130/0016-7606(1975)86<273:hmffdi>2.0.co;2

Guo, L., Zhang, H.-F., Harris, N., Xu, W.-C., & Pan, F.-B. (2017). Detrital zircon U–Pb geochronology, trace-element and Hf isotope geochemistry of the metasedimentary rocks in the Eastern Himalayan syntaxis: Tectonic and paleogeographic implications. *Gondwana Research*, *41*, 207–221. https://doi.org/10.1016/j.gr.2015.07.013

Haproff, P. J., Zuza, A. V., & Yin, A. (2018). West-directed thrusting south of the eastern Himalayan syntaxis indicates clockwise crustal flow at the indenter corner during the India-Asia collision. *Tectonophysics*, *722*, 277–285. https://doi.org/10.1016/j.tecto.2017.11.001

Holbourn, A., Kuhnt, W., Regenberg, M., Schulz, M., Mix, A., & Andersen, N. (2010). Does Antarctic glaciation force migration of the tropical rain belt? *Geology*, *38*(9), 783–786. https://doi.org/10.1130/g31043.1

Hu, P.-Y., Zhai, Q.-G., Zhao, G.-C., Wang, J., Tang, Y., Zhu, Z.-C., & Wu, H. (2019). The North Lhasa terrane in Tibet was attached with the Gondwana before it was drafted away in Jurassic: Evidence from detrital zircon studies. *Journal of Asian Earth Sciences*, *185*, 104055. https://doi.org/10.1016/j.jseaes.2019.104055

Ingersoll, R. V., Dickinson, W. R., & Graham, S. A. (2003). *Remnant-ocean submarine fans: Largest sedimentary systems on Earth*. https://doi.org/10.1130/0-8137-2370-1.191

Jain, A. K., Lal, N., Sulemani, B., Awasthi, A. K., Singh, S., Kumar, R., & Kumar, D. (2009). Detrital-zircon fission-track ages from the Lower Cenozoic sediments, NW Himalayan foreland basin: Clues for exhumation and denudation of the Himalaya during the India-Asia collision. *GSA Bulletin*, *121*(3–4), 519–535. https://doi.org/10.1130/b26304.1

Jain, A. K., Takur, V. C., & Tandon, S. K. (1974). Stratigraphy and structure of the Siang District, Arunachal (NEFA) Himalaya. *Himalayan Geology*, *4*, 28–60.

Johnson, S. Y., & Alam, A. M. N. (1991). Sedimentation and tectonics of the Sylhet trough, Bangladesh. *Geological Society of America Bulletin*, *103*, 1513–1527. https://doi.org/10.1130/0016-7606(1991)103<1513:satots>2.3.co;2

Krishna, K. S., Ismaiel, M., Srinivas, K., Gopala Rao, D., Mishra, J., & Saha, D. (2016). Sediment pathways and emergence of Himalayan source material in the Bay of Bengal. *Current Science*, *110*(3), 363. https://doi.org/10.18520/cs/v110/i3/363-372

Kumar, G. (1997). *Geology of Arunachal Pradesh* (Vol. 217). GSI.

Lalnuntluanga, P. (2013). *Magnetostratigraphic studies of the Surma and Tipam groups in parts of the Kolasib District, Mizoram*. PhD Thesis. Mizoram University.thesis

Lalnuntluanga, P., Malsawma, J., Lalremruatfela, C., Tiwari, R. P., & Sangode, S. J. (2014). Correlation of four magnetostratigraphically constrained sections of Miocene Bhuban Formation of Surma Basin in Mizoram, India. In *Indian Miocene: A geodynamic and chronologic framework for paleobiota, sedimentary environments, and paleoclimates: Paleontological Society of India, special publication* (Vol. 5, pp. 87–100).

Lalremruatfela, C. (2020). *Magnetostratigraphic study of Barail group in Champhai District, Mizoram*. PhD Thesis. Government Zirtiri Residencial Science College.thesis

Lang, K. A., & Huntington, K. W. (2014). Antecedence of the Yarlung–Siang–Brahmaputra River, eastern Himalaya. *Earth and Planetary Science Letters*, *397*, 145–158. https://doi.org/10.1016/j.epsl.2014.04.026

Lang, K. A., Huntington, K. W., Burmester, R., & Housen, B. (2016). Rapid exhumation of the eastern Himalayan syntaxis since the late Miocene. *Bulletin of the Geological Society of America*, *128*(9–10), 1403–1422. https://doi.org/10.1130/b31419.1

Laskowski, A. K., Kapp, P., & Cai, F. (2018). Gangdese culmination model: Oligocene–Miocene duplexing along the India-Asia suture zone, Lazi region, southern Tibet. *GSA Bulletin*, *130*(7–8), 1355–1376. https://doi.org/10.1130/b31834.1

Laskowski, A. K., Kapp, P., Ding, L., Campbell, C., & Liu, X. (2017). Tectonic evolution of the Yarlung suture zone, Lopu Range region, southern Tibet. *Tectonics*, *36*(1), 108–136. https://doi.org/10.1002/2016tc004334

Leary, R., Orme, D. A., Laskowski, A. K., DeCelles, P. G., Kapp, P., Carrapa, B., & Dettinger, M. (2016). Along-strike diachroneity in deposition of the Kailas Formation in central southern Tibet: Implications for Indian slab dynamics. *Geosphere*, *12*(4), 1198–1223. https://doi.org/10.1130/ges01325.1

Li, G., Sandiford, M., Liu, X., Xu, Z., Wei, L., & Li, H. (2014). Provenance of Late Triassic sediments in central Lhasa terrane, Tibet and its implication. *Gondwana Research*, *25*(4), 1680–1689. https://doi.org/10.1016/j.gr.2013.06.019

Liebke, U., Antolin, B., Appel, E., Basavaiah, N., Mikes, T., Dunkl, I., & Wemmer, K. (2011). Indication for clockwise rotation in the Siang window south of the eastern Himalayan syntaxis and new geochronological constraints for the area. *Geological Society, London, Special Publications*, *353*(1), 71–97. https://doi.org/10.1144/sp353.5

Lindsay, J. F., Holliday, D. W., & Hulbert, A. G. (1991). Sequence stratigraphy and the evolution of the Ganges-Brahmaputra delta complex. *American Association of Petroleum Geologists Bulletin*, *75*(7), 1233–1254. https://doi.org/10.1306/0c9b291b-1710-11d7-8645000102c1865d

Long, S. P., McQuarrie, N., Tobgay, T., Coutand, I., Cooper, F. J., Reiners, P. W., et al. (2012). Variable shortening rates in the eastern Himalayan thrust belt, Bhutan: Insights from multiple thermochronologic and geochronologic data sets tied to kinematic reconstructions. *Tectonics*, *31*(5), TC5004. https://doi.org/10.1029/2012tc003155

Mallick, R., Hubbard, J. A., Lindsey, E. O., Bradley, K. E., Moore, J. D. P., Ahsan, A., et al. (2020). Subduction initiation and the rise of the Shillong Plateau. *Earth and Planetary Science Letters*, *543*, 116351. https://doi.org/10.1016/j.epsl.2020.116351

Malsawma, J., Lalnuntluanga, P., Badekar, A., Tiwari, R. P., & Sangode, S. J. (2010). Magnetic polarity stratigraphy of the Bhuban succession, Surma Group, Tripura-Mizoram accretionary belt. *Journal of the Geological Society of India*, *76*, 119–133. https://doi.org/10.1007/s12594-010-0086-9

Maurin, T., & Rangin, C. (2009). Structure and kinematics of the Indo-Burmese Wedge: Recent and fast growth of the outer wedge. *Tectonics*, *28*(2), 1–21. https://doi.org/10.1029/2008tc002276

McNeill, L. C., Dugan, B., Backman, J., Pickering, K. T., Pouderoux, H. F. A., Henstock, T. J., et al. (2017). Understanding Himalayan erosion and the significance of the Nicobar Fan. *Earth and Planetary Science Letters*, *475*, 134–142. https://doi.org/10.1016/j.epsl.2017.07.019

McQuarrie, N., Eizenhöfer, P. R., Long, S. P., Tobgay, T., Ehlers, T. A., Blythe, A. E., et al. (2019). The influence of foreland structures on hinterland cooling: Evaluating the drivers of exhumation in the Eastern Bhutan Himalaya. *Tectonics*, *38*(9), 3282–3310. https://doi.org/10.1029/2018tc005340

Métivier, F., Gaudemer, Y., Tapponnier, P., & Klein, M. (1999). Mass accumulation rates in Asia during the Cenozoic. *Geophysical Journal International*, *137*(2), 280–318. https://doi.org/10.1046/j.1365-246X.1999.00802.x

Miller, K. G., Kominz, M. A., Browning, J. V., Wright, J. D., Mountain, G. S., Katz, M. E., et al. (2005). The Phanerozoic record of global sea-level change. *Science*, *310*(5752), 1293–1298. https://doi.org/10.1126/science.1116412

Milliman, J. D., & Farnsworth, K. L. (2011). *River discharge to the coastal ocean: A global synthesis*. Cambridge University Press.

Mitra, S., Priestley, K. F., Borah, K., & Gaur, V. K. (2018). Crustal Structure and Evolution of the Eastern Himalayan Plate Boundary System, Northeast India. *Journal of Geophysical Research: Solid Earth*, *123*(1), 621–640. https://doi.org/10.1002/2017jb014714

Najman, Y. (2006). The detrital record of orogenesis: A review of approaches and techniques used in the Himalayan sedimentary basins. *Earth-Science Reviews*, *74*(1), 1–72. https://doi.org/10.1016/j.earscirev.2005.04.004

Najman, Y., Allen, R., Willett, E. A. F., Carter, A., Barfod, D., Garzanti, E., et al. (2012). The record of Himalayan erosion preserved in the sedimentary rocks of the Hatia Trough of the Bengal Basin and the Chittagong Hill Tracts, Bangladesh. *Basin Research*, *24*(5), 499–519. https://doi.org/10.1111/j.1365-2117.2011.00540.x

Najman, Y., Bickle, M., BouDagher-Fadel, M., Carter, A., Garzanti, E., Paul, M., et al. (2008). The Paleogene record of Himalayan erosion: Bengal Basin, Bangladesh. *Earth and Planetary Science Letters*, *273*(1), 1–14. https://doi.org/10.1016/j.epsl.2008.04.028

Najman, Y., Bracciali, L., Parrish, R. R., Chisty, E., & Copley, A. (2016). Evolving strain partitioning in the Eastern Himalaya: The growth of the Shillong Plateau. *Earth and Planetary Science Letters*, *433*, 1–9. https://doi.org/10.1016/j.epsl.2015.10.017

Najman, Y., Carter, A., Oliver, G., & Garzanti, E. (2005). Provenance of Eocene foreland basin sediments, Nepal: Constraints to the timing and diachroneity of early Himalayan orogenesis. *Geology*, *33*(4), 309–312. https://doi.org/10.1130/g21161.1

Najman, Y., Mark, C., Barfod, D. N., Carter, A., Parrish, R., Chew, D., & Gemignani, L. (2019). Spatial and temporal trends in exhumation of the Eastern Himalaya and syntaxis as determined from a multitechnique detrital thermochronological study of the Bengal Fan. *GSA Bulletin*, 1–16. https://doi.org/10.1130/b35031.1

Nandy, D. R. (1999). *Tectono-geological map of north-eastern India and adjoining region* (Map). Geological Survey of Indiamap.

Nandy, D. R. (2001). *Geodynamics of northeastern India and the adjoining region*. ACB Publications.

Ni, J. F., Guzman-Speziale, M., Bevis, M., Holt, W. E., Wallace, T. C., & Seager, W. R. (1989). Accretionary tectonics of Burma and the three-dimensional geometry of the Burma subduction zone. *Geology*, *17*(1), 68. https://doi.org/10.1130/0091-7613(1989)017<0068:atobat>2.3.co;2

Palin, R. M., Searle, M. P., St-Onge, M. R., Waters, D. J., Roberts, N. M. W., Horstwood, M. S. A., et al. (2015). Two-stage cooling history of pelitic and semi-pelitic mylonite (sensu lato) from the Dongjiu–Milin shear zone, northwest flank of the eastern Himalayan syntaxis. *Gondwana Research*, *28*(2), 509–530. https://doi.org/10.1016/j.gr.2014.07.009

Pickering, J. L., Goodbred, S. L., Reitz, M. D., Hartzog, T. R., Mondal, D. R., & Hossain, M. S. (2014). Late Quaternary sedimentary record and Holocene channel avulsions of the Jamuna and Old Brahmaputra River valleys in the upper Bengal delta plain. *Geomorphology*, *227*, 123–136. https://doi.org/10.1016/j.geomorph.2013.09.021

Pickering, K. T., Carter, A., Andò, S., Garzanti, E., Limonta, M., Vezzoli, G., & Milliken, K. L. (2020). Deciphering relationships between the Nicobar and Bengal submarine fans, Indian Ocean. *Earth and Planetary Science Letters*, *544*, 116329. https://doi.org/10.1016/j.epsl.2020.116329

Pickering, K. T., Pouderoux, H., McNeill, L. C., Backman, J., Chemale, F., Kutterolf, S., et al. (2020). Sedimentology, stratigraphy and architecture of the Nicobar fan (Bengal–Nicobar fan system), Indian Ocean: Results from international ocean discovery program expedition 362. *Sedimentology*, *67*(5), 2248–2281. https://doi.org/10.1111/sed.12701

Pilgrim, G. E. (1913). The correlation of the Siwaliks with the mammal horizons of Europe. *Records of the Geological Survey of India*, *43*, 264–325.

Pullen, A., Ibáñez-Mejía, M., Gehrels, G. E., Ibáñez-Mejía, J. C., & Pecha, M. (2014). What happens when n= 1000? Creating large-n geochronological datasets with LA-ICP-MS for geologic investigations. *Journal of Analytical Atomic Spectrometry*, *29*(6), 971–980. https://doi.org/10.1039/c4ja00024b

Ranga Rao, A. (1983). Geology and hydrocarbon potential of a part of Assam-Arakan Basin and its adjacent region. In Bhandari, L. L., Venkatachala, B. S., Kumar, R., Swamy, S. N., Garga, P., and Srivastava, D. C. (Ed.), *Petroliferous basins of India* (Vol. 6, pp. 112–127). Petroleum Asia Journal.

Rangin, C., Maurin, T., & Masson, F. (2013). Combined effects of Eurasia/Sunda oblique convergence and East-Tibetan crustal flow on the active tectonics of Burma. *Journal of Asian Earth Sciences*, *76*, 185–194. https://doi.org/10.1016/j.jseaes.2013.05.018

Raymo, M. E., & Ruddiman, W. F. (1992). Tectonic forcing of late Cenozoic climate. *Nature*, *359*(6391), 117–122. https://doi.org/10.1038/359117a0

Robinson, R. A. J., Brezina, C. A., Parrish, R. R., Horstwood, M. S. A., Win Oo, N., Bird, M. I., et al. (2014). Large rivers and orogens: The evolution of the Yarlung Tsangpo-Irrawaddy system and the eastern Himalayan syntaxis. *Gondwana Research*, *26*(1), 112–121. https://doi.org/10.1016/j.gr.2013.07.002

Roy, B., Roy, S., Goyal, K., Ghosh, S., & Sanyal, P. (2021). Biomarker and carbon isotopic evidence of marine incursions in the Himalayan foreland basin during its overfilled stage. *Paleoceanography and Paleoclimatology*, *36*(5), e2020PA004083. https://doi.org/10.1029/2020pa004083

Salvi, D., Mathew, G., Pande, K., & Kohn, B. P. (2021). Phased cooling of the Siang antiform, Eastern Himalaya: Insight from multi-thermochronology and thermal studies. *Journal of Earth System Science*, *130*(1), 45. https://doi.org/10.1007/s12040-020-01541-7

Sawant, S. S., Vijaya Kumar, K. V., Balaram, V., Rao, S. D., Rao, K. S., & Tiwari, R. P. (2017). Geochemistry and genesis of craton-derived sediments from active continental margins: Insights from the Mizoram Foreland Basin, NE India. *Chemical Geology*, *470*, 13–32. https://doi.org/10.1016/j.chemgeo.2017.08.020

Saylor, J. E., & Sundell, K. E. (2016). Quantifying comparison of large detrital geochronology data sets. *Geosphere*, *12*(1), 203–220. https://doi.org/10.1130/ges01237.1

Sincavage, R., Betka, P. M., Thomson, S. N., Seeber, L., Steckler, M., & Zoramthara, C. (2020). Neogene shallow-marine and fluvial sediment dispersal, burial, and exhumation in the ancestral Brahmaputra delta: Indo-Burman Ranges, India. *Journal of Sedimentary Research*, *90*, 1244–1263. https://doi.org/10.2110/jsr.2020.60

Sincavage, R., Goodbred, S., & Pickering, J. (2018). Holocene Brahmaputra River path selection and variable sediment bypass as indicators of fluctuating hydrologic and climate conditions in Sylhet Basin, Bangladesh. *Basin Research*, *30*(2), 302–320. https://doi.org/10.1111/bre.12254

Singh, A., Bhushan, K., Singh, C., Steckler, M. S., Akhter, S. H., Seeber, L., et al. (2016). Crustal structure and tectonics of Bangladesh: New constraints from inversion of receiver functions. *Tectonophysics*, *680*, 99–112. https://doi.org/10.1016/j.tecto.2016.04.046

Steckler, M. S., Akhter, S. H., & Seeber, L. (2008). Collision of the Ganges–Brahmaputra Delta with the Burma Arc: Implications for earthquake hazard. *Earth and Planetary Science Letters*, *273*(3), 367–378. https://doi.org/10.1016/j.epsl.2008.07.009

Steckler, M. S., Mondal, D. R., Akhter, S. H., Seeber, L., Feng, L., Gale, J., et al. (2016). Locked and loading megathrust linked to active subduction beneath the Indo-Burman Ranges. *Nature Geoscience*, *9*(8), 615–618. https://doi.org/10.1038/ngeo2760

Stewart, R. J., Hallet, B., Zeitler, P. K., Malloy, M. A., Allen, C. M., & Trippett, D. (2008). Brahmaputra sediment flux dominated by highly localized rapid erosion from the easternmost Himalaya. *Geology*, *36*(9), 711. https://doi.org/10.1130/g24890a.1

Stickroth, S. F., Carrapa, B., DeCelles, P. G., Gehrels, G. E., & Thomson, S. N. (2019). Tracking the growth of the Himalayan fold-and-thrust belt from lower Miocene foreland basin strata: Dumri formation, western Nepal. *Tectonics*, *38*(11), 3765–3793. https://doi.org/10.1029/2018tc005390

Sundell, K. E., & Saylor, J. E. (2017). Unmixing detrital geochronology age distributions. *Geochemistry, Geophysics, Geosystems*, *18*(8), 2872–2886. https://doi.org/10.1002/2016gc006774

Thura Tun, S., Maung Thein, Nyunt Htay, & Kyaing Sein (2014). *Geological map of Myanmar 1:2,250,000*.

Tiwari, R. P., & Kachhara, R. P. (2003). Molluscan biostratigraphy of the Tertiary sediments of the Mizoram, India. *Journal of the Palaeontological Society of India*, *48*, 65–88. http://www.palaeontologicalsociety.in/vol48/v4.pdf

Uddin, A., Hames, W. E., & Zahid, K. M. (2010). Laser40Ar/39Ar age constraints on Miocene sequences from the Bengal basin: Implications for middle Miocene denudation of the eastern Himalayas. *Journal of Geophysical Research*, *115*(B7), B07416. https://doi.org/10.1029/2009jb006401

Uddin, A., & Lundberg, N. (1999). A paleo-Brahmaputra? Subsurface lithofacies analysis of Miocene deltaic sediments in the Himalayan–Bengal system, Bangladesh. *Sedimentary Geology*, *123*(3–4), 239–254. https://doi.org/10.1016/s0037-0738(98)00134-1

Vadlamani, R., Wu, F.-Y., & Ji, W.-Q. (2015). Detrital zircon U–Pb age and Hf isotopic composition from foreland sediments of the Assam Basin, NE India: Constraints on sediment provenance and tectonics of the Eastern Himalaya. *Journal of Asian Earth Sciences*, *111*, 254–267. https://doi.org/10.1016/j.jseaes.2015.07.011

Vermeesch, P. (2013). Multi-sample comparison of detrital age distributions. *Chemical Geology*, *341*, 140–146. https://doi.org/10.1016/j.chemgeo.2013.01.010

Vermeesch, P. (2018). IsoplotR: A free and open toolbox for geochronology. *Geoscience Frontiers*, *9*(5), 1479–1493. https://doi.org/10.1016/j.gsf.2018.04.001

Vernant, P., Bilham, R., Szeliga, W., Drupka, D., Kalita, S., Bhattacharyya, A. K., et al. (2014). Clockwise rotation of the Brahmaputra Valley relative to India: Tectonic convergence in the eastern Himalaya, Naga Hills, and Shillong Plateau. *Journal of Geophysical Research: Solid Earth*, *119*(8), 6558–6571. https://doi.org/10.1002/2014jb011196

Wang, Q., Zhu, D.-C., Cawood, P. A., Chung, S.-L., & Zhao, Z.-D. (2021). Resolving the paleogeographic puzzle of the Lhasa Terrane in southern Tibet. *Geophysical Research Letters*, *48*(15), e2021GL094236. https://doi.org/10.1029/2021gl094236

Wang, Y., Sieh, K., Tun, S. T., Lai, K.-Y., & Myint, T. (2014). Active tectonics and earthquake potential of the Myanmar region: Active Tectonics of Myanmar. *Journal of Geophysical Research: Solid Earth*, *119*(4), 3767–3822. https://doi.org/10.1002/2013jb010762

White, N. M., Pringle, M., Garzanti, E., Bickle, M., Najman, Y., Chapman, H., & Friend, P. (2002). Constraints on the exhumation and erosion of the High Himalayan Slab, NW India, from foreland basin deposits. *Earth and Planetary Science Letters*, *195*(1), 29–44. https://doi.org/10.1016/s0012-821x(01)00565-9

Yang, L., Xiao, W., Julleh Jalalur Rahman, M., Windley, B. F., Schulmann, K., Ao, S., et al. (2018). Provenance of the Cenozoic Bengal Basin sediments: Insights from U-Pb ages and Hf isotopes of detrital zircons. *Geological Journal*, 1–13. https://doi.org/10.1002/gj.3258

Yang, X., Groeneveld, J., Jian, Z., Steinke, S., & Giosan, L. (2020). Middle Miocene intensification of south Asian monsoonal rainfall. *Paleoceanography and Paleoclimatology*, *35*(12), e2020PA003853. https://doi.org/10.1029/2020pa003853

Yin, A., Dubey, C. S., Kelty, T. K., Webb, A. A. G., Harrison, T. M., Chou, C. Y., & Célérier, J. (2010). Geologic correlation of the Himalayan orogen and Indian craton: Part 2. Structural geology, geochronology, and tectonic evolution of the Eastern Himalaya. *Geological Society of America Bulletin*, *122*(3–4), 360–395. https://doi.org/10.1130/b26461.1

Yin, A., Dubey, C. S., Webb, A. A. G., Kelty, T. K., Grove, M., Gehrels, G. E., & Burgess, W. P. (2010). Geologic correlation of the Himalayan orogen and Indian craton: Part 1. Structural geology, U-Pb zircon geochronology, and tectonic evolution of the Shillong Plateau and its neighboring regions in NE India. *GSA Bulletin*, *122*(3–4), 336–359. https://doi.org/10.1130/b26460.1

Zachos, J., Pagani, M., Sloan, L., Thomas, E., & Billups, K. (2001). Trends, rhythms, and aberrations in global climate 65 Ma to present. *Science*, *292*(5517), 686–693. https://doi.org/10.1126/science.1059412

Zeitler, P. K., Meltzer, A. S., Brown, L., Kidd, W. S. F., Lim, C., & Enkelmann, E. (2014). *Tectonics and topographic evolution of Namche Barwa and the easternmost Lhasa block, Tibet*. https://doi.org/10.1130/2014.2507(02)

Zhu, D., Wang, Q., Cawood, P. A., Zhao, Z., & Mo, X. (2017). Raising the Gangdese Mountains in southern Tibet. *Journal of Geophysical Research: Solid Earth*, *122*(1), 214–223. https://doi.org/10.1002/2016jb013508

Zhu, D.-C., Zhao, Z.-D., Niu, Y., Dilek, Y., & Mo, X.-X. (2011). Lhasa terrane in southern Tibet came from Australia. *Geology*, *39*(8), 727–730. https://doi.org/10.1130/g31895.1

References From the Supporting Information

Bernet, M., & Garver, J. I. (2005). Fission-track analysis of detrital zircon. *Reviews in Mineralogy and Geochemistry*, *58*(1), 205–237. https://doi.org/10.2138/rmg.2005.58.8

Galbraith, R. F., & Laslett, G. M. (1993). Statistical models for mixed fission track ages. *Nuclear Tracks and Radiation Measurements*, *21*(4), 459–470. https://doi.org/10.1016/1359-0189(93)90185-c

Gehrels, G., & Pecha, M. (2014). Detrital zircon U-Pb geochronology and Hf isotope geochemistry of Paleozoic and Triassic passive margin strata of western North America. *Geosphere*, *10*(1), 49–65. https://doi.org/10.1130/GES00889.1

Gehrels, G., Valencia, V., & Pullen, A. (2006). Detrital zircon geochronology by laser-ablation multicollector ICPMS at the Arizona LaserChron Center. *Paleontological Society Papers*, *12*, 67–76. https://doi.org/10.1017/s1089332600001352

Gehrels, G. E., Valencia, V. A., & Ruiz, J. (2008). Enhanced precision, accuracy, efficiency, and spatial resolution of U-Pb ages by laser ablation-multicollector-inductively coupled plasma-mass spectrometry. *Geochemistry, Geophysics, Geosystems*, *9*(3), Q03017. https://doi.org/10.1029/2007gc001805

Gleadow, A. J. W. (1981). Fission-track dating methods: What are the real alternatives? *Nuclear Tracks and Radiation Measurements*, *5*(1), 3–14. https://doi.org/10.1016/0191-278x(81)90021-4

Gleadow, A. J. W., Hurford, A. J., & Quaife, R. D. (1976). Fission track dating of zircon: Improved etching techniques. *Earth and Planetary Science Letters*, *33*(2), 273–276. https://doi.org/10.1016/0012-821x(76)90235-1

Hurford, A. J. (1990). Standardization of fission track dating calibration: Recommendation by the Fission Track Working Group of the I.U.G.S. Subcommission on Geochronology. *Chemical Geology: Isotope Geoscience section*, *80*, 171–178. https://doi.org/10.1016/0168-9622(90)90025-8

Hurford, A. J., & Green, P. F. (1983). The zeta age calibration of fission-track dating. *Chemical Geology*, *41*, 285–317. https://doi.org/10.1016/s0009-2541(83)80026-6

Ludwig, K. R. (2008). *Isoplot 3.60* (Vol. 4). Berkeley Geochronology Center.

Stacey, J. S., & Kramers, J. D. (1975). Approximation of terrestrial lead isotope evolution by a two-stage model. *Earth and Planetary Science Letters*, *26*(2), 207–221. https://doi.org/10.1016/0012-821x(75)90088-6

Erratum

In the originally published version of this article, two references (Bretschneider, Hathorne, Bolton, et al., 2021; Bretschneider, Hathorne, Huang, et al., 2021) were missing in the reference section and as in-text citations in the second to last sentence of Section 5.3, paragraph 2. The references are now added to the article. This may be considered the authoritative version of record.